Land degradation monitoring and assessment

ESA–MOST China Dragon 4 Cooperation

2019 ADVANCED INTERNATIONAL TRAINING COURSE IN LAND REMOTE SENSING

中欧科技合作“龙计划”第四期 2019年陆地遥感高级培训班

18 to 23 November 2019 | Chongqing University, P.R. China

培训时间:2019年11月18日-23日 主办方:重庆大学

Land degradation monitoring and assessment

Prof. Gao Zhihai & Dr. Bin Sun

Institute of Forest Resource Information Techniques (IFRIT),

Chinese Academy of Forestry (CAF)

Nov. 22th，2019

IFRIT

Contents

1 Definitions and reviews

Land degradation is a process that land productive capacity continues to decline or even lose completely under the influence of natural forces and human activities.

- **Desertification in drylands is an important problem world-wide, but the concept is ambiguous in terms of specific processes, conditions, and solutions.**
- **UNCCD: Persistent and severe reductions in biological productivity due to unsustainable land uses in drylands, often associated with climatic and societal factors such as poverty and migration.**

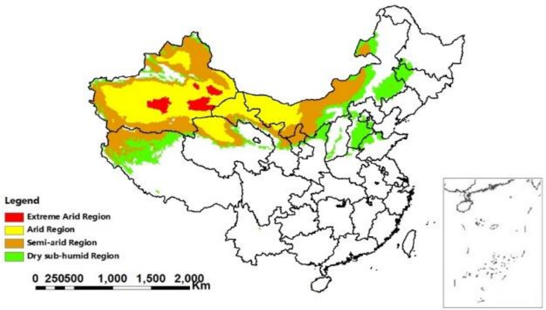

Scope of the general potential extent of desertification in China（1981-2010）

Diverse types of land degradation and desertification

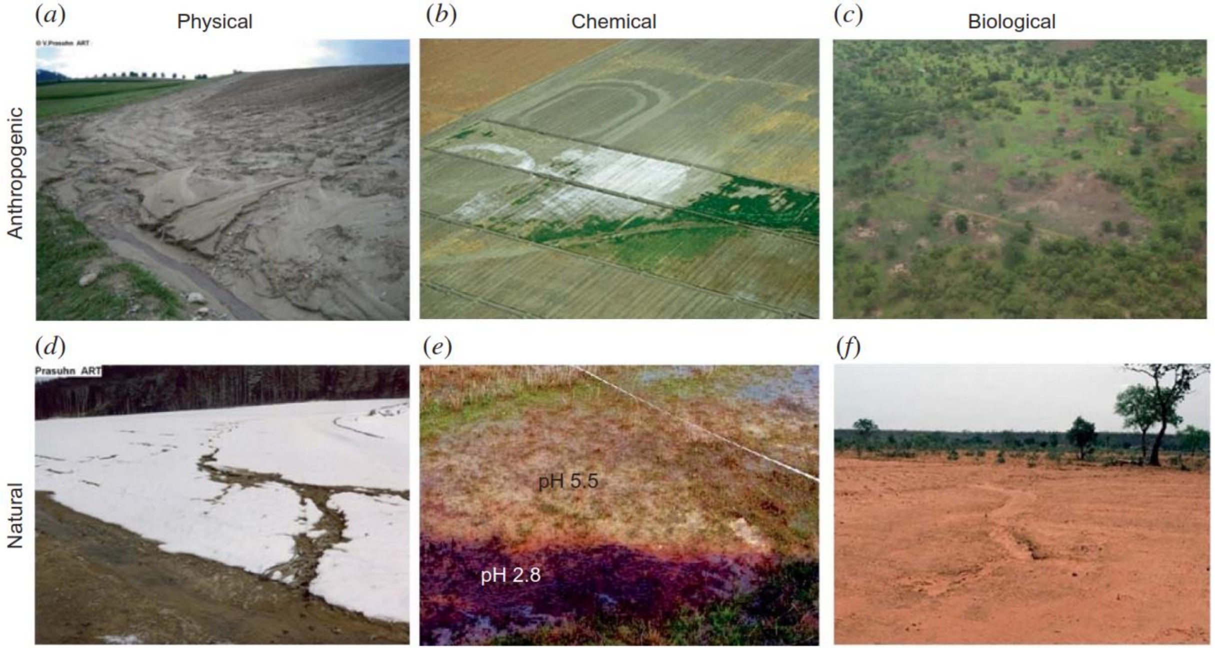

Figure 1. Examples of land degradation. (*a*) Man-induced soil erosion on agricultural fields (Volker Prasuhn, website); (*b*) secondary (man-induced) salinity in farmland, California (USDA Agricultural Research Service); (*c*) loss of forest cover through shifting agriculture, Wau district, Sudan (UNEP website); (*d*) soil erosion induced by snowmelt (Volker Prasuhn); (*e*) acid sulphate scald caused by drainage change (Gardner *et al.* 2004), which may be natural or man-made; and (*f*) drought-induced vegetation decline and soil erosion (WMO).

Regions sensitive to desertification

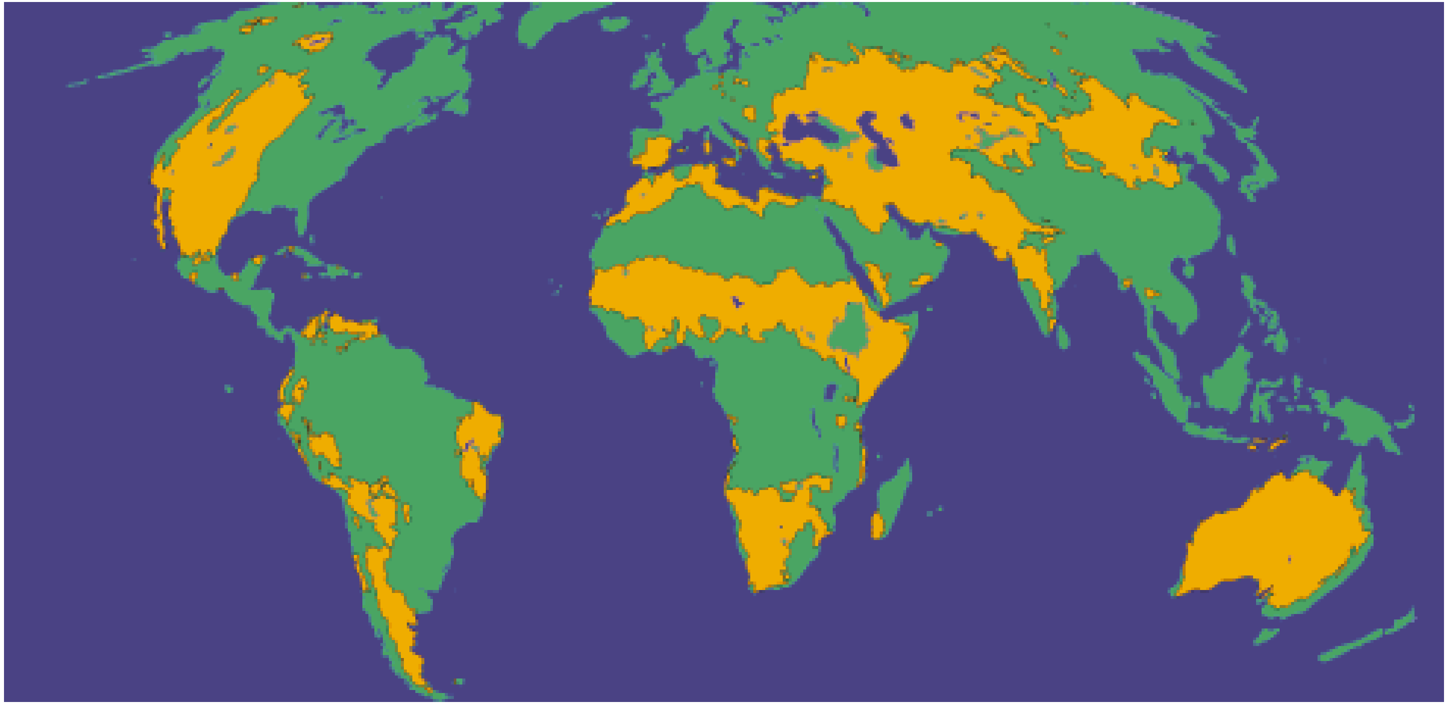

Dryland regions of the world (yellow), cover about 54 million km^2, amounts to 40% of the global land area.

2002/GEF/UNEP/FAO/（LADA）

1991/UNEP/（GLASOD）

1992/UNEP（WAD1）

1997/UNEP/（WAD2）

2018/EU/（WAD3）

2007/UNEP/（GEO4）

2018/IPBES

●●●

Overall situation of land degradation

- 1991，Global Assessment of Human-induced Soil Degradation，GLASOD(**Expert interpretation, 12 classes);** ASSOD, **Relative degradation**(FAO,UNEP,UNDP)
- 1992，World Atlas of Desertification (First edition)(GLASOD,GLADIS),UNEP
- 1997，World Atlas of Desertification (Second edition),UNEP
- 2002，Land Degradation Assessment in Drylands，LADA;GLADA;GLADIS
- 2007，Global Environment Outlook 4, UNEP
- 2018，World Atlas of Desertification (Third edition),EU
- 2018，The Assessment Report on Land Degradation and Restoration,IPBES

◆ Vegetatior … certain extent by vegetat … fluctuation
◆ Areas of d … fied accurately … getation parameter

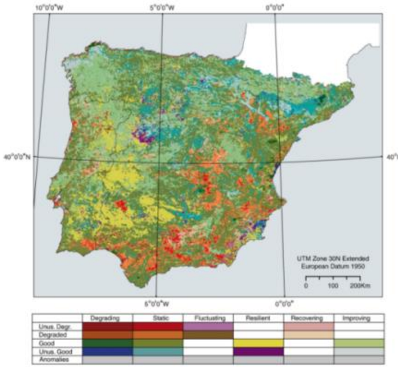

GLADA

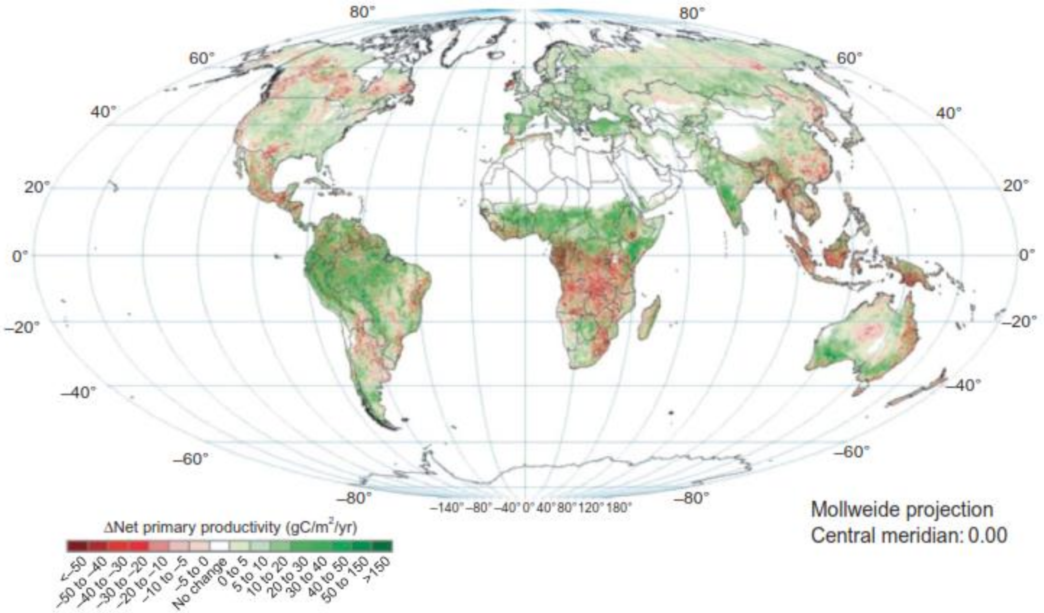

Figure 4. Linear trends in net primary production (NPP) from the global assessment of land degradation and improvement (GLADA). Reproduced from Bai *et al.* (2008).

Contents

2.Desertification status in China

Desertification： land degradation in arid, semi-arid and dry sub-humid areas.

Harms： About a quarter of the global land is affected by desertification hazards. China is one of the most seriously affected countries by desertification.

Causes:

(1)Climatic variation：Climatic change, drought…

(2)Human activities: over-grazing, over-reclamation, mismanagement of water resources etc.

Climatic Types of Desertification in China

Climate Type	Moisture Index (MI)
Extreme arid area*	MI ≦ 0.05
Arid area	0.05< MI < 0.20
Semi-arid area	0.20< MI < 0.50
Dry sub-humid area	0.50< MI < 0.65
Sub-humid and Humid area*	MI > 0.65

*Means the climate scope without possible occurrence of desertification

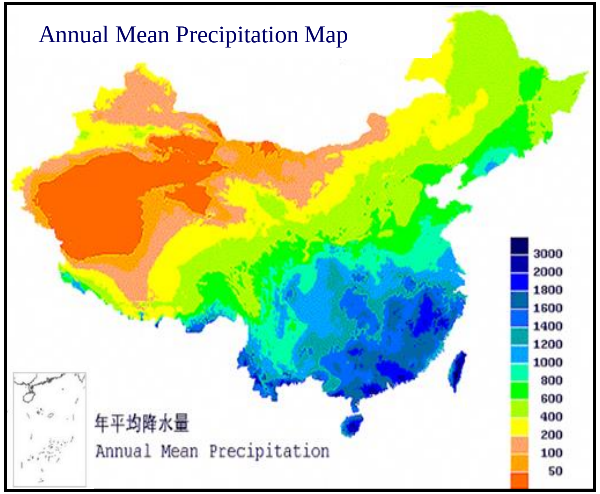

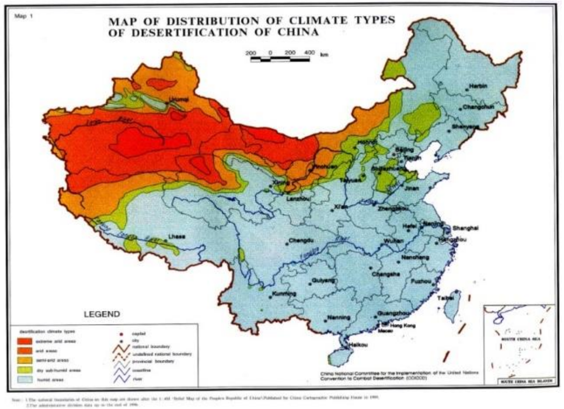

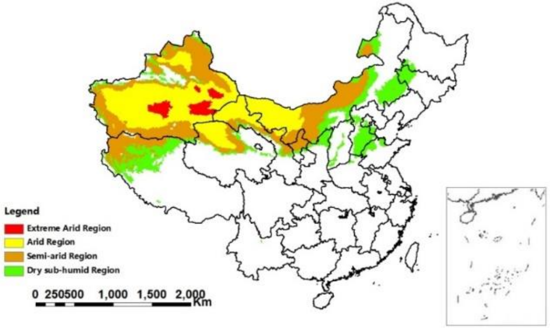

Moisture Index (MI)— Calculated with the Thornthwaite method (UNCCD)

$$MI = P/E_0$$

$$E_0 = 16(10T/I)^a$$

$$a = (0.675I - 77.1I^2 + 17920I + 492390) \times 10^{-6}$$

$$I = \sum (T/5)^{1.514}$$

$$APE = E_0 \times CF$$

P: precipitation (mm), E_0: potential evapotranspiration (PE, mm), T: monthly temperature (°C), I: annual thermal index, APE: modified PE (mm), CF: coefficient of sunshine hours varied with latitudes.

Land Use/Cover Types of Desertification

(1) Cropland;

(2) Rangeland & pastures;

(3) Woodlands & Forest;

(4) Resident settlements & industry/transport facilities and mining areas;

(5) Waste lands.

Desertification Types

(1) Caused by wind erosion: in sandy areas of North, Northwest and Northeast China

(2) Caused by water erosion: in Loess of Plateau of North and Northwest China and some mountainous areas

(3) Caused by soil salinization or alkilization: in Northwest and Northeast China

(4) Caused by Freezing and thawing processes: in Tibet Plateau

(5) Caused by other interacted factors.

Grading of Severity of Desertification

(1) Slight desertification

(2) Medium desertification

(3) Severe desertification

Sandy desertification and sandstorm

Soil and water erosion in Loess Plateau

Salinization In Hexi corridor, Gansu

Tree planting

Sandy Desertification Control

straw checkerboard barriers

Sandy Desertification Control

Control of water erosion

Terraced farmlands in Loess Plateau

Vegetation recovery in a small watershed of the Loess Plateau

Desertification Monitoring

Definition: Monitoring of desertification is to detect the dynamic changes of desertified lands and inherent mechanical change of desertification process within a defined spatial and temporal area with practical measures, to understand the developing process and grading stage of desertification.

Significances:

a) Providing data for establishing national pre-alarming and forecasting system of desertification disaster;
b) Framing the national policies for combating desertification;
c) Distributing projects for combating desertification.

Resolutions

Spectral resolution: the specific wavelength intervals that are a sensor can record;

Spatial resolution: the area on the ground represented by each pixel;

Radiometric resolution: the number of possible data file value in each band (indicated by bit);

Temporal resolution: how often a sensor obtains imagery of a particular area.

Remotely Sensed Data

Airborne data

Early stages: 1950-1970's, plastic films or photo copy;

Modern stage: 1980's - , digital data, Higher spatial & spectral resolutions.

Spaceborne data (Satellite data)

Multispectral data: NOAA, MODIS, CBERS-1/2, Beijing-1, HJ-1A/B, Landsat MSS/TM/ETM, EO-1 ALI, SPOT-4/5, etc;

Hyperspectral data: PROBA CHRIS, EO-1 Hyperion, HJ-1A, etc。

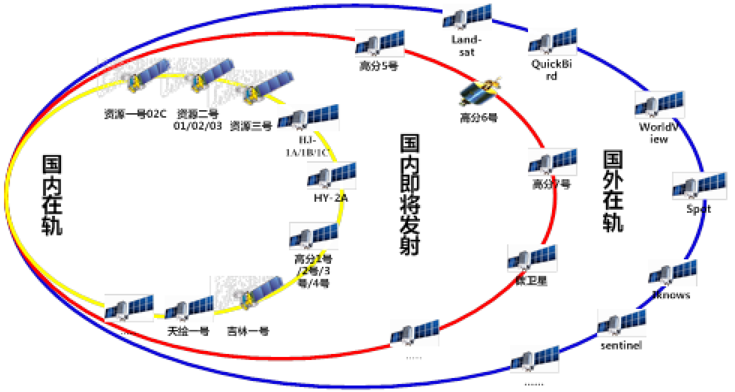

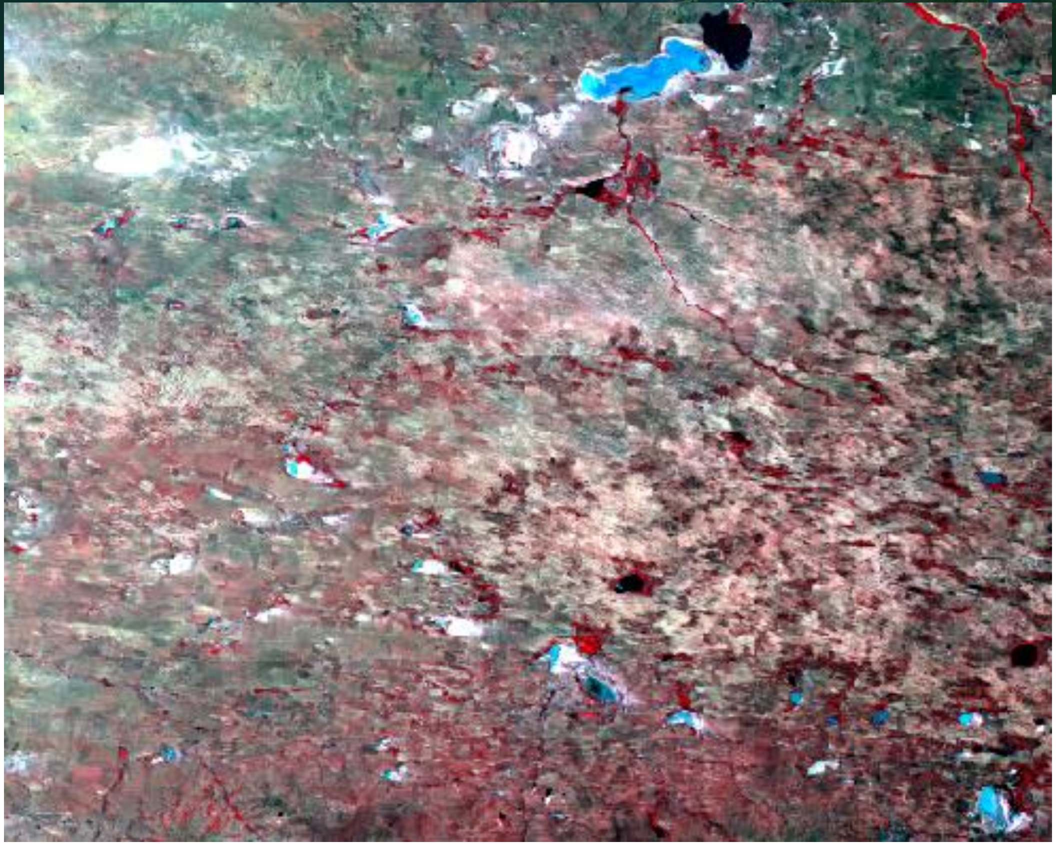

GF-1 16m data
（Otindag sandy land）
April 26, 2013

GF-1 multispectral image (16m)

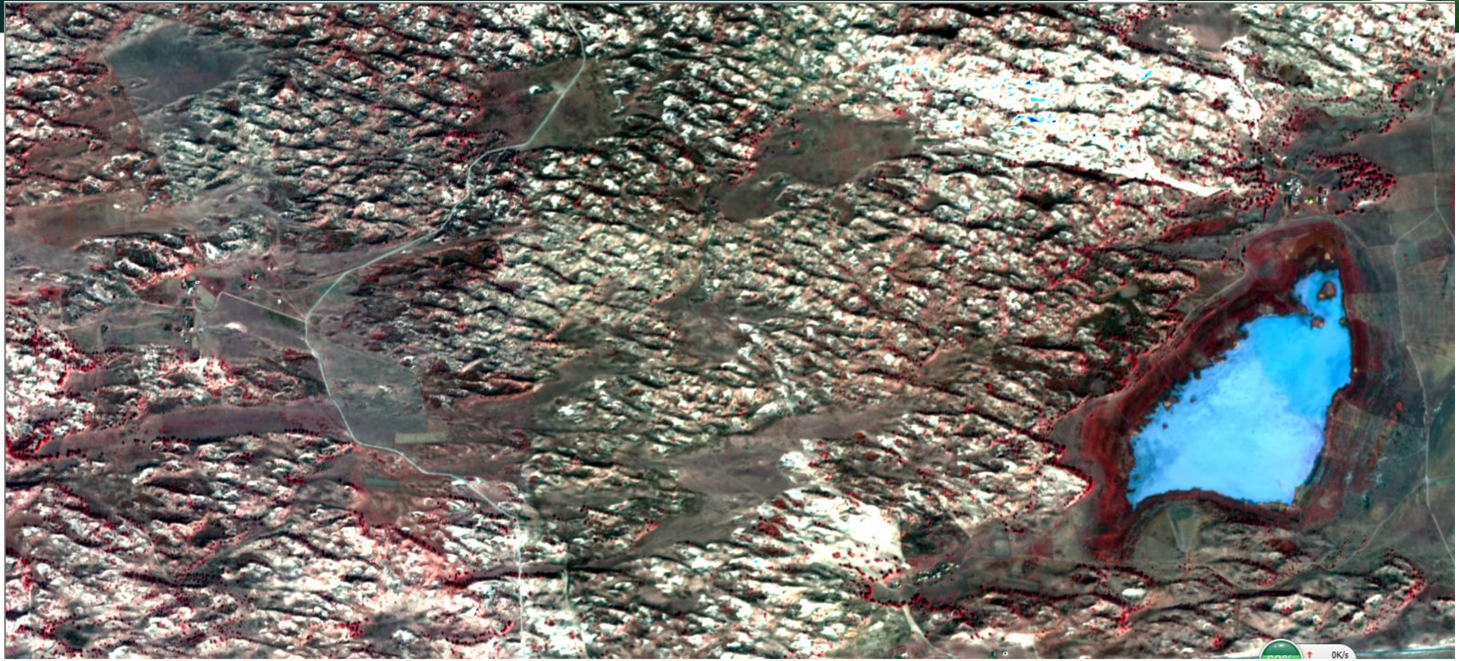

GF-2 Multispectral images（Otindag sandy land）
August 19, 2014

GF-2 Multispectral and panchromatic images（Minqin, Gansu）

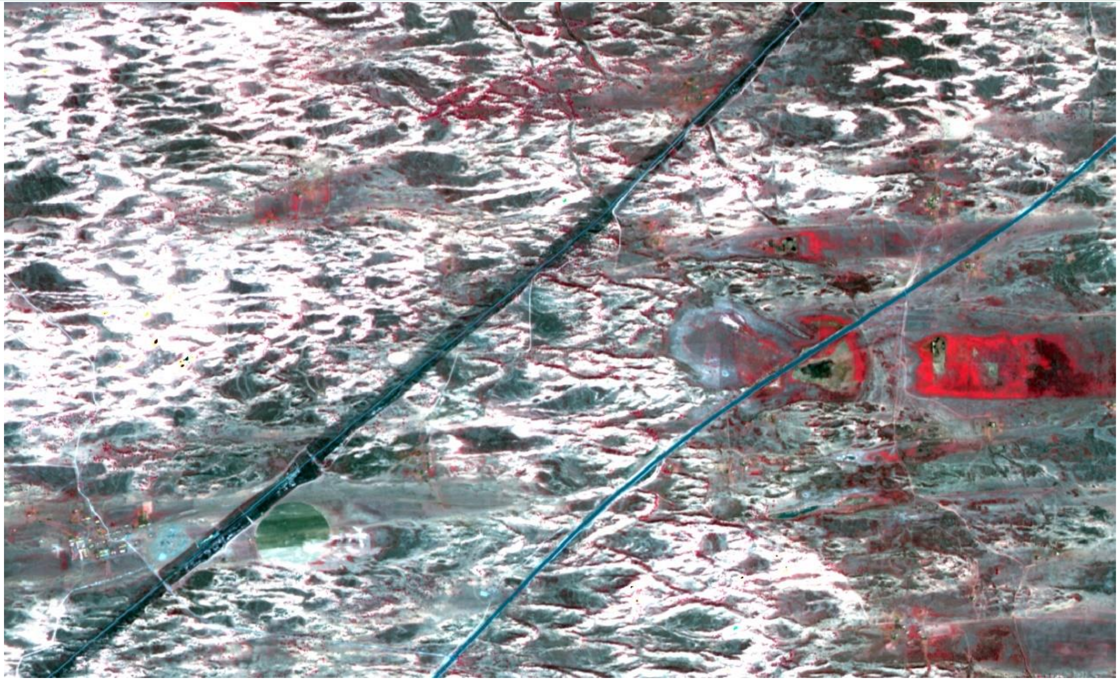

ZY-3 Multispectral images
（Otindag sandy land）
January 9, 2012


TM

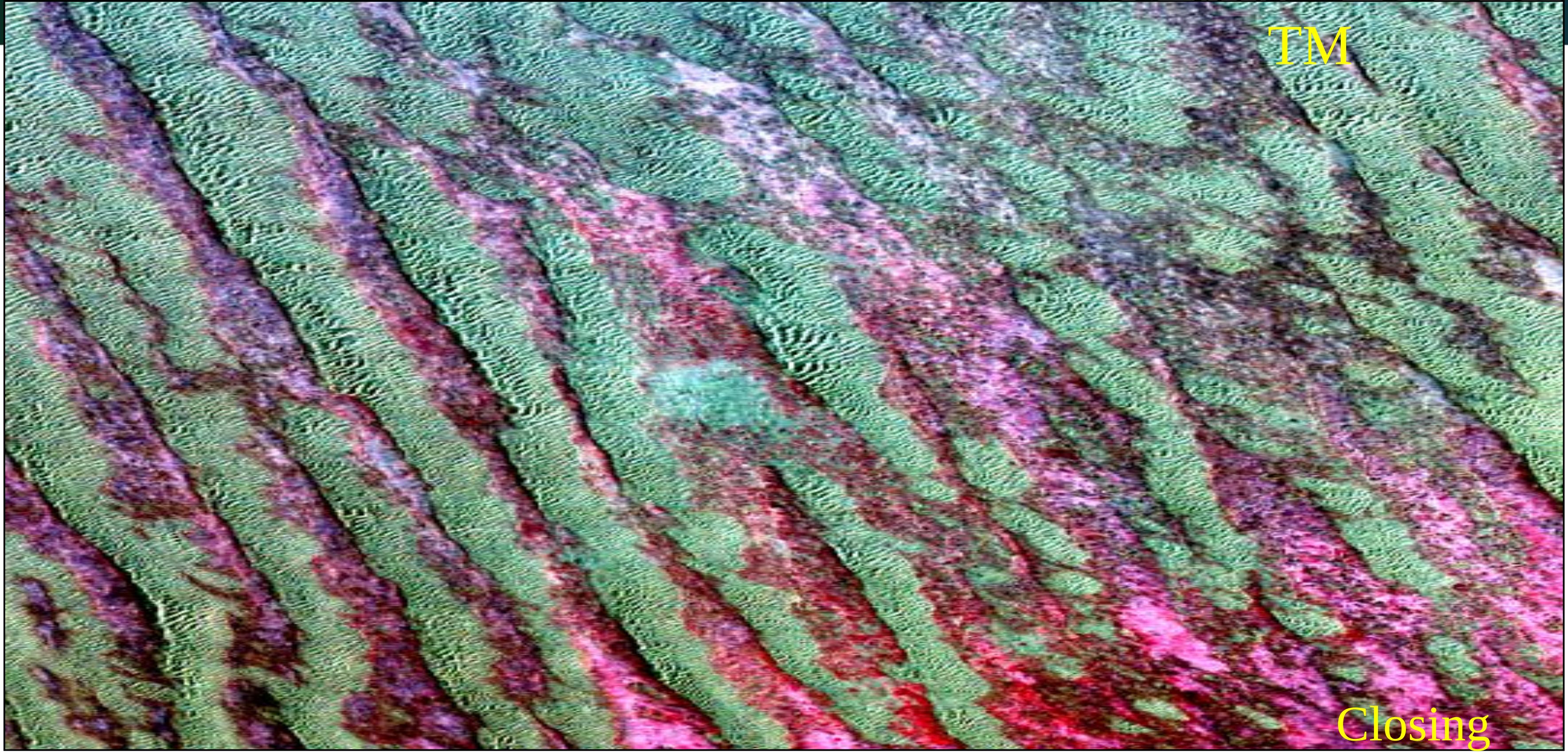
TM
Closing

Rapideye

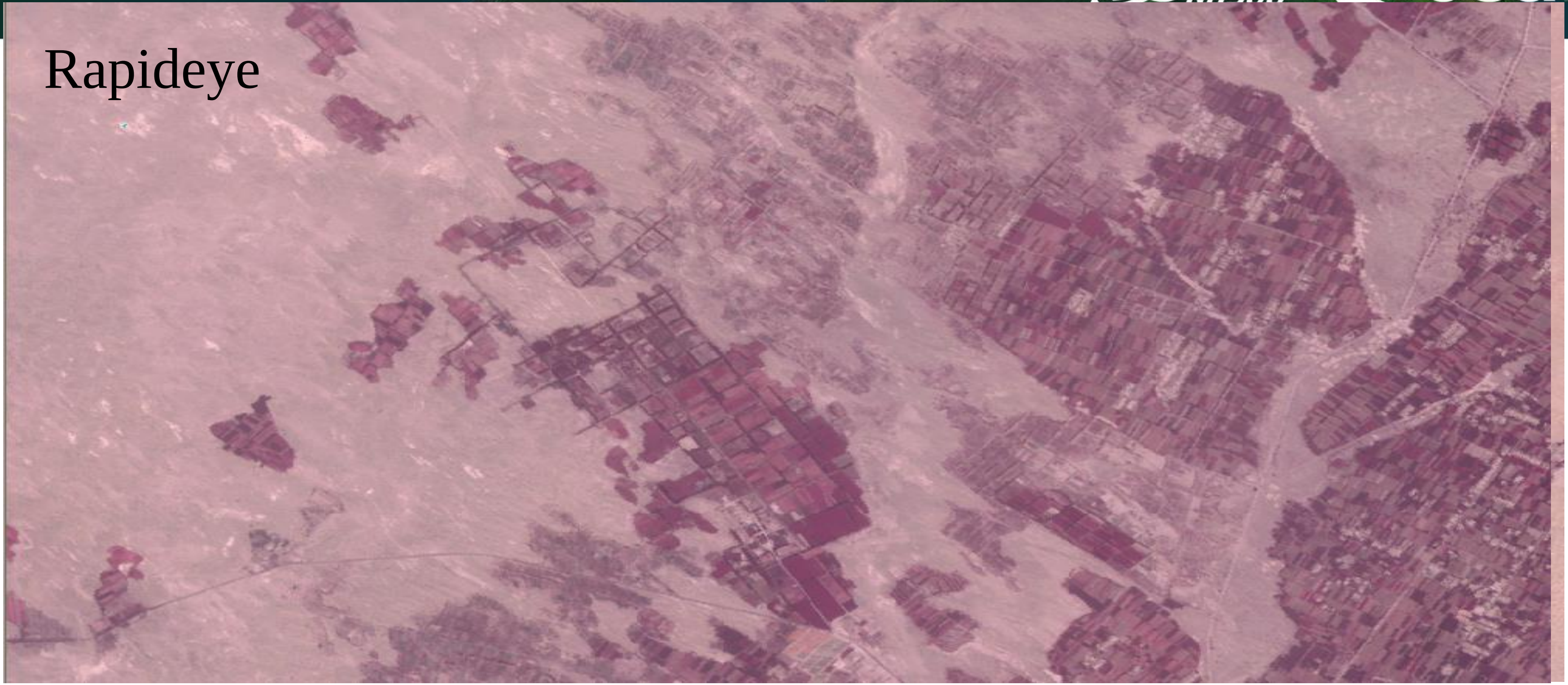

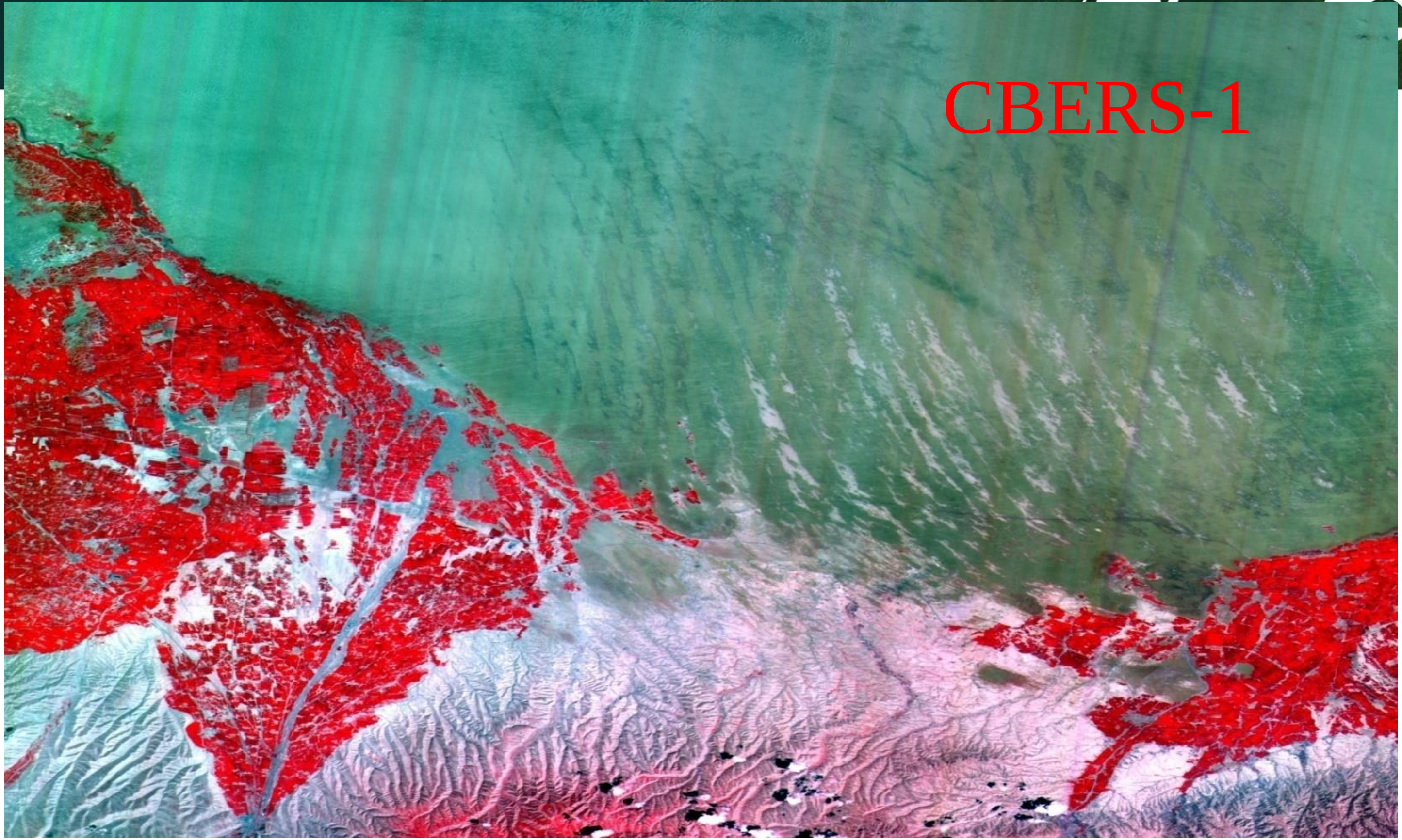
CBERS-1

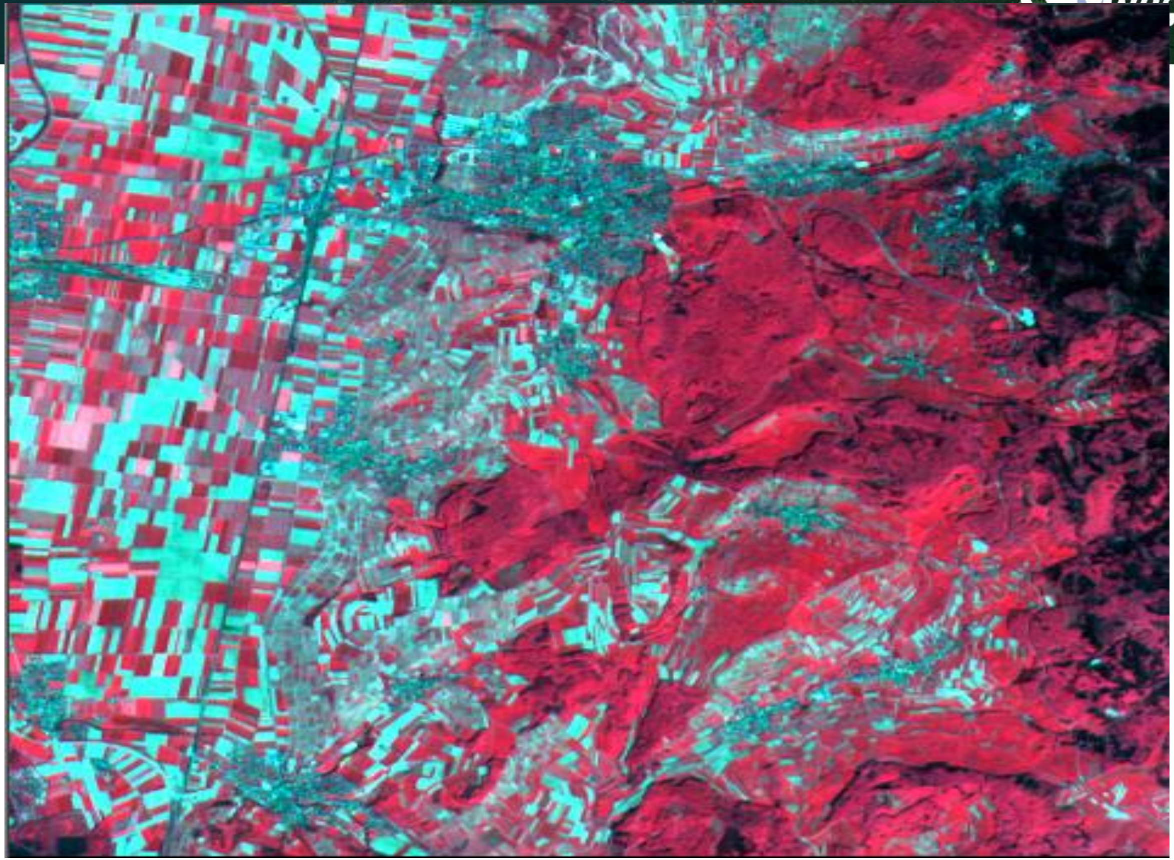

SPOT-5

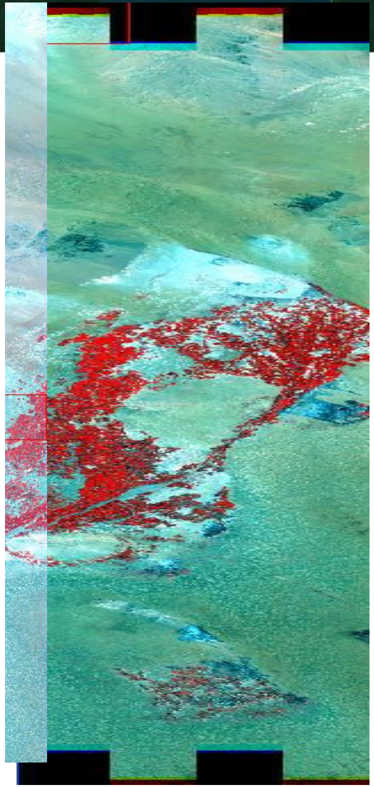

EO-1 HYPERION

EO-1 ALI

National Desertification Monitoring in China

Five times of ***The national desertification and sandification monitoring*** have been organized with integration of remote sensing and in situ survey from 1994 to 2014.

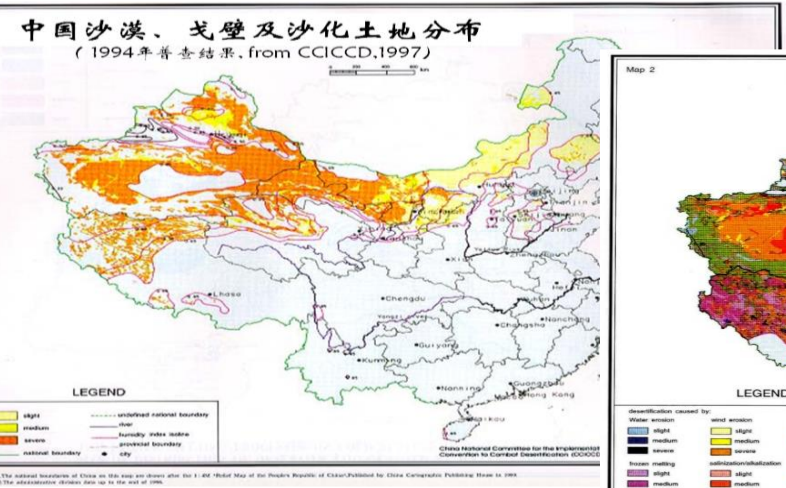

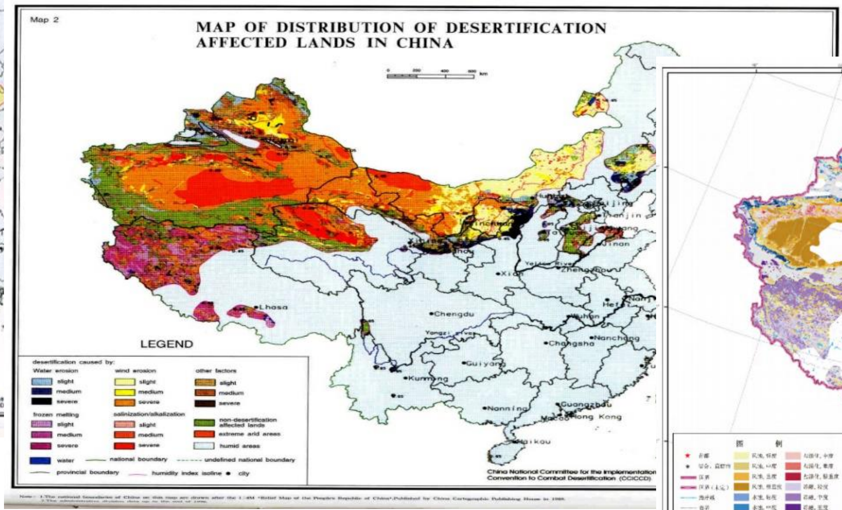

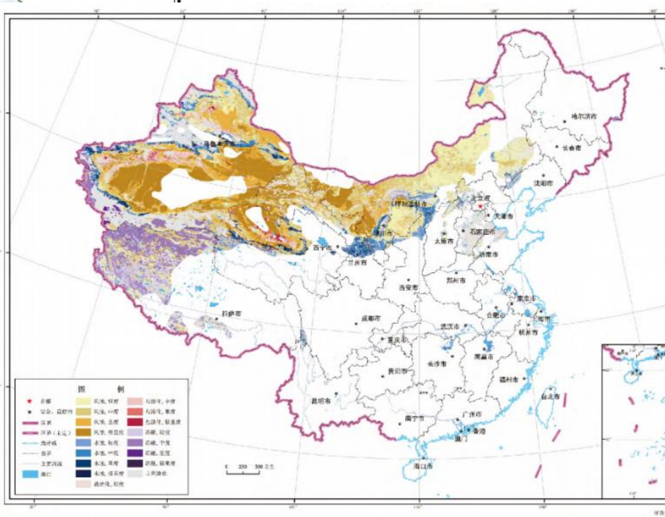

Flow Chart of National Desertification & Sandification Monitoring (NDM)

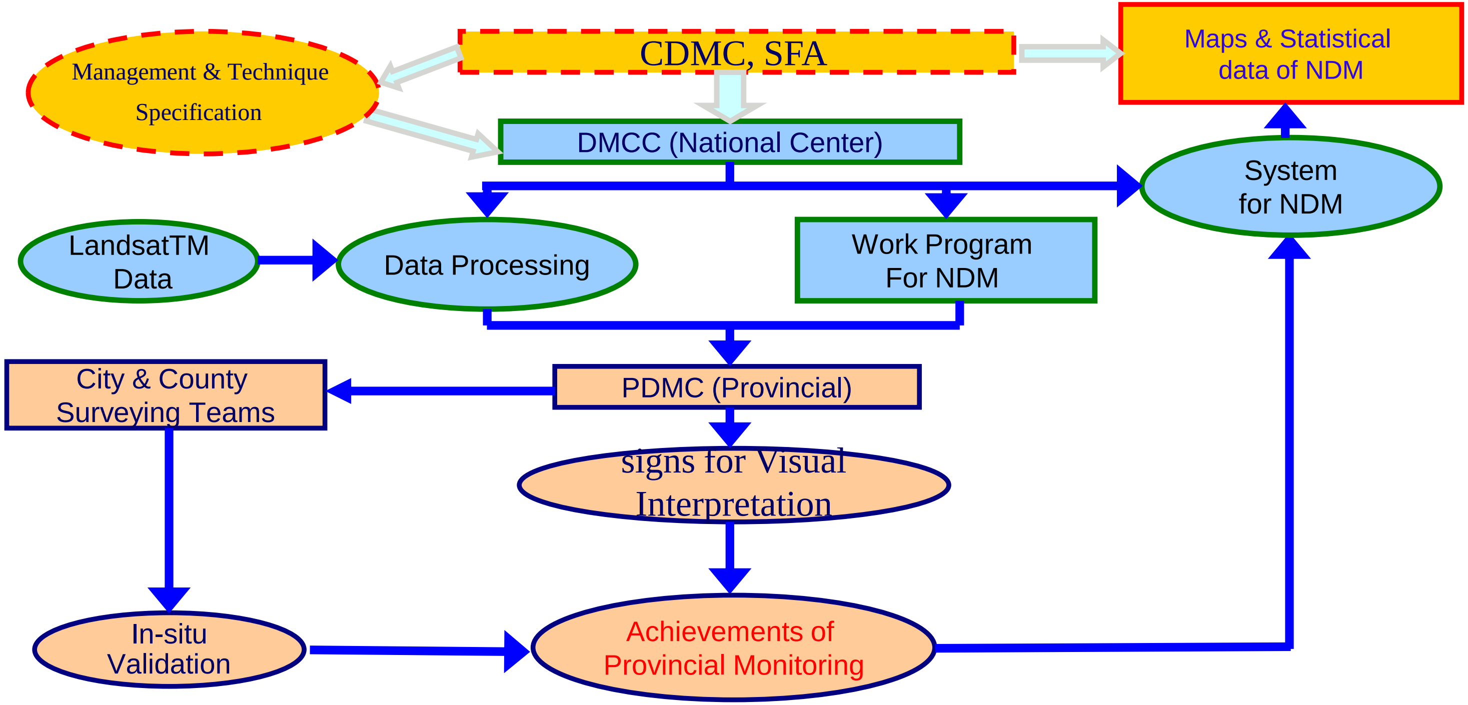

Desertification Indicator System

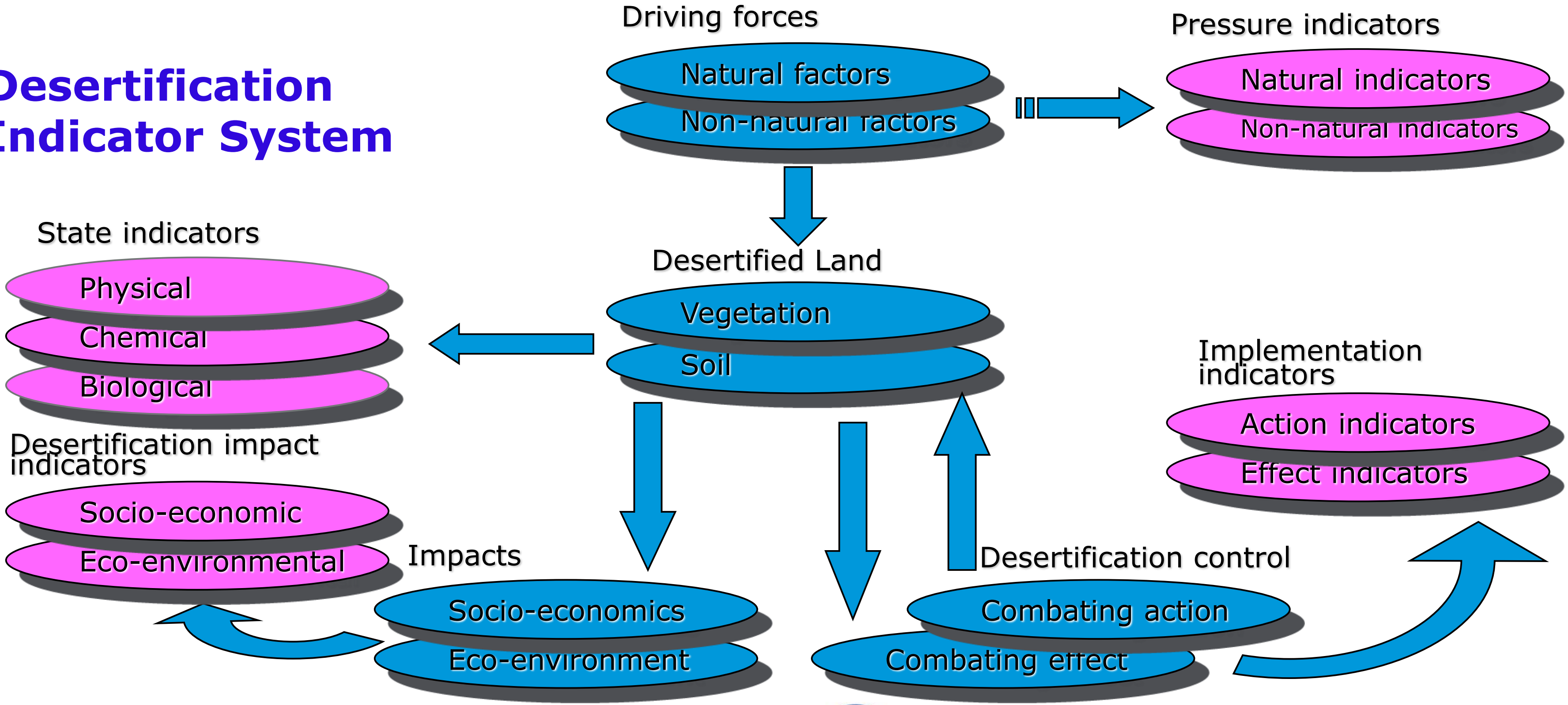

Grading indicators of various desertification

- **Desertification caused by wind erosion**

✓ **Slight:**

Vegetation cover is >30%;

Land surface is covered by stable dunes or sandy field,

Water-leakage sandy land;

Cultivated fields transformed from sandy land.

- **Medium:**

Vegetation cover is between 10% and 30%, and is evenly distributed;

Sand drift are under control by plant community;

Sand movement ripples are prevailing on sand dunes or sand fields.

- **Severe:**

The surface is composed of Gobi;

Vegetation cover is less than 10%;

Sand dunes are stabilized with non-biological measures;

Surface landform is composed of denuded residuals, unfertilized fields, Yardang landforms, clay mounds and wind blowouts.

Table 2. Indicators for grading severity of desertification caused by water erosion

Severity	Erosion Modulus ($t/km^2.a$)	Mean annual loss Depth (mm)
Slight	1000 -2500	2
Medium	2500 -8000	2-6
Severe	> 8 000	> 6

- **Desertification caused by water erosion**

Table 3. Indicators for grading the severity of desertification caused by frozen and melting processes at cold plateau

Severity	Locations of the occurrence of desertification
Slight	Extreme highlands, high mountains, gentle slope meadow and flooded depression and ridge area on plateau.
Medium	Extreme highlands, high & cold hills and desert steppe.
Severe	Extreme highlands, high mountains, high & cold mountain deserts and cold deserts.

- **Desertification caused by frozen and melting**

Desertification caused by Soil salinization

Table 4. Soil salinization classification & grading indicators

Type	0-30 cm salt content (%)		
	West Region (Xinjiang)	East Region (Inner Mongolia)	Reclam possibility
Slight	0.5-1.0	0.1-0.3	With favorable conditions to be reclaimed by simple improvement only
Medium	1.0-1.5	0.3-0.7	water conservancy project and improvement measurement are required.
Severe	1.5-2.0	0.7-1.0	Reclaim condition is poor& integrated measures needed.

Desertification and Sandification Areas from 1994 to 2014

Inventoried Year	Desertification Area（M km²）	Wind Erosion Area（M km²）	Sandification Area（M km²）
1994	2.622	1.607	1.714
1999	2.674	1.873	1.743
2004	2.636	1.839	1.740
2009	2.624	1.832	1.731
2014	2.611	1.826	1.721

Issues and challenges

(1) Indicators for desertification monitoring and assessment;

(2) Thresholds of indicators proposed;

(3) Bench mark of Desertification

(4) Quantitative inversion of the surface parameters by remote sensing.

Contents

Contents

3.1 PV/NPV estimation

3.2 Sandy Land detection by Spectral Mixture Analysis

3.3 Estimating AGB by using EO data and ML

3 Extraction of Desertification Information from Remote Sensing data

3.1 PV/NPV estimation

- Vegetation coverage, a key indicator of desertification. Remote sensing offers a unique opportunity for the retrieval at large scale.
- From a functional perspective, vegetation could be divided into PV(green leaves) and NPV(wood, senescent material, litter). PV, well studied, based on difference in visible and NIR reflectance. NPV estimation receives less attention, because of spectral similarity with soils.
- It is wroth noting that NPV widely existed in arid and semi-arid regions, and play a key role in controlling wind and water erosion. Thus, estimating fractional coverage of PV and NPV simultaneously is very important for desertification monitoring in drylands.
- **Examining the performance of different SMA techniques in estimating the fractional cover of PV and NPV simultaneously in relation to in *situ* fractional cover measurements, with GF-1 WFV data(only visible and NIR bands), in a complex landscape , the Otinday sandy land**

3.1.1 Study Area- Otindag sandy land

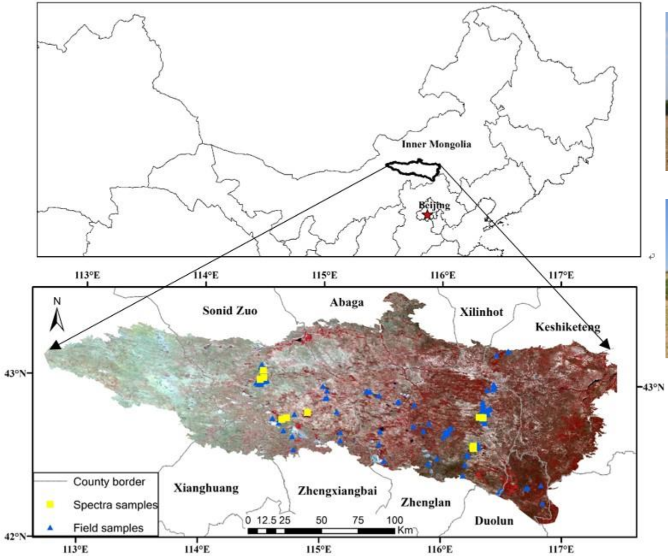

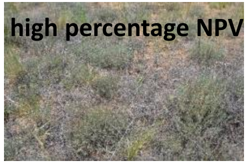

- **semi-arid area, strong wind, less precipitation.**
- **Because of desertification process, most grasslands have experienced different degrees of shrub encroachment.**
- **The NPV account for a high percentage and vary seasonally and inter-annually.**

3.1.2 Data acquisition

Remote Sensing Data

■**Radiometric correction:** DN value was converted to radiance using the calibration coefficients obtained from the CRESDA.

■**Atmospheric correction:** Radiance was transformed to surface reflectance through FLAASH algorithm provided by ENVI 5.0.

■**Geometric correction:** Landsat-8 OLI data provided by USGS, proved geometrically consistent with the field GPS values, were selected as the base map for geometric correction (ENVI 5.0). The geometric correction error was less than one pixel of the Landsat-8 pan data (15m).

5 GF-1 WFV scenes, from 3 cameras

Sensor	Acquisition date	Seriel number
WFV3	2014/07/31	291592
WFV3	2014/07/31	291593
WFV4	2014/07/31	291607
WFV4	2014/07/31	291608
WFV2	2014/08/04	294882

http://www.cresda.com/

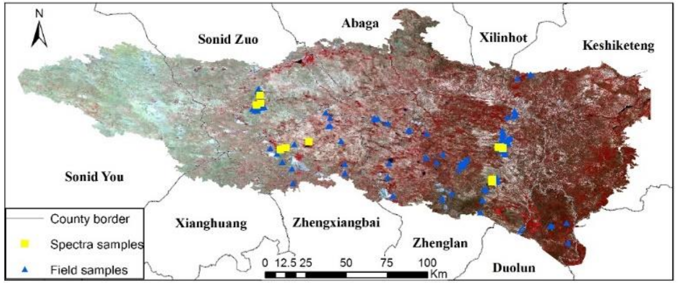

Field Spectra

- **Device:** ASD full-range (350-2500 nm) Fieldspec® 4.
- **Methods:** Collected within 2 hour of local solar noon on clear sky days. The sensor, held 1m above the top of the PV, NPV or bare soil surface in vertical downward position.
- **Acquired spectra:** Synchronous with GF-1 data acquisition, 29 PV spectra, 14 NPV spectra and 12 bare soil spectra were measured. For acquiring more NPV spectra, 14 NPV spectra and 3 bare soil spectra were acquired in November.
- **Pre-process:** Based on the spectral response function of GF-1 WFV sensor, the field spectra were resampled to the GF-1 WFV bands.

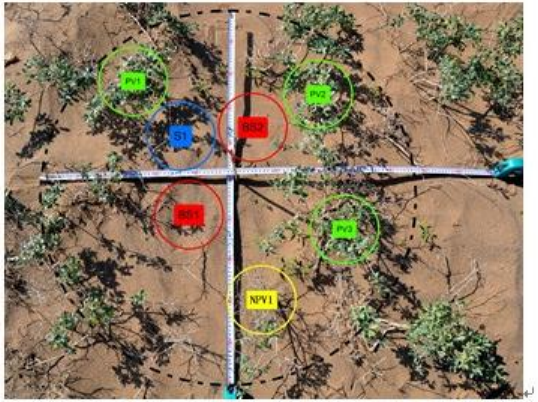

■**Time:** late July and early August, season of max vegetation cover.

■**Sample design:**121 sites were selected ,based on stratified random design and accessibility, one 32×32 m plot was set up in each site.

■**Methods:** Along the 2 or 3 transects, the surveyors recorded the cover type (PV, NPV, SOIL) at 1m interval directly under a thin tape. Vegetation is divided into three categories: non-woody or ground cover; woody less than 2 meters; and woody greater than 2 meters.

■**Position:** The coordinates of the cross point of two transects were recorded by GPS to match with GF-1 WFV data

In *situ* data

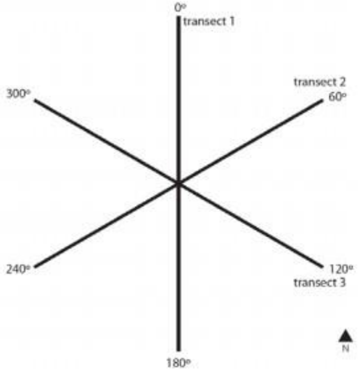

Natural vegetation

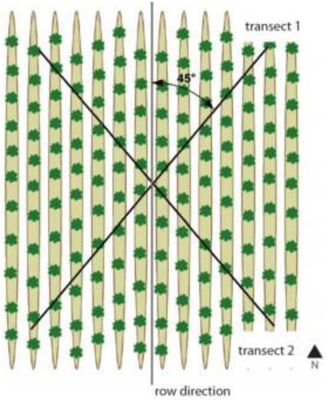

Artificial vegetation

3.1.3 Method

SMA methods adopted(Linear)

Reflectance of a pixel is assumed to be a linear combination of the reflectance of the spectra of the EMs, weighted by their fractional cover.

- **Traditional SMA**
  - Fixed EMs, the average spectra of PV, NPV and bare soil were utilized as the EM spectra.
- **MESMA**
  - All EM combinations are calculated, the best-fit model (lowest RMSE) is determined for each pixel.
- **AutoMCU**
  - A large number of EM combinations for each pixel are calculated by randomly selecting spectra from a spectral library. Assumed f*cover* distributed normally, when the number of EM combinations are sufficient, the average value of f*cove*r would be taken as the final results.

Unmixing approach

Three approaches are different in EM selection. For the calculation of f_k in each time, the Fully Constrained Least Square (FCLS) algorithm would be applied. Through using FCLS, two important constraints on f_k :

- fraction sum-to-one constraint (ASC) $\sum_{k=1}^{n} f_k = 1$
- fraction nonnegativity constraint (ANC) $f_k \geq 0$

Performance assessment

To compare the performance of different SMA techniques on PV/NPV fractional cover estimation, two metrics were calculated against in *situ* data, RMSE and coefficient of determination (R^2) of linear regression.

$$\mathrm{RMSE} = \sqrt{\sum_{i=1}^{n}(x_i - y_i)^2 / n}$$

$$R^2 = \frac{\sum_{i=1}^{n}(x_i-\bar{x})(y_i-\bar{y})^2}{\sum_{i=1}^{n}(x_i-\bar{x})^2 \sum_{i=1}^{n}(y_i-\bar{y})^2}$$

EM library and variability

- **General:** **PV spectra is easily distinguishable from NPV and bare soil spectra, but the NPV and bare soil are similarly.**
- **Differences between BS and NPV:** **Higher reflectance of BS, mainly due to the extensive bright sandy substrate. Bow-shaped protuberance existed for BS, while not emerging in NPV.**
- **Intra-variability:** **The PV and NPV spectra are relatively concentrated, while the bare soil spectra varies greatly.**

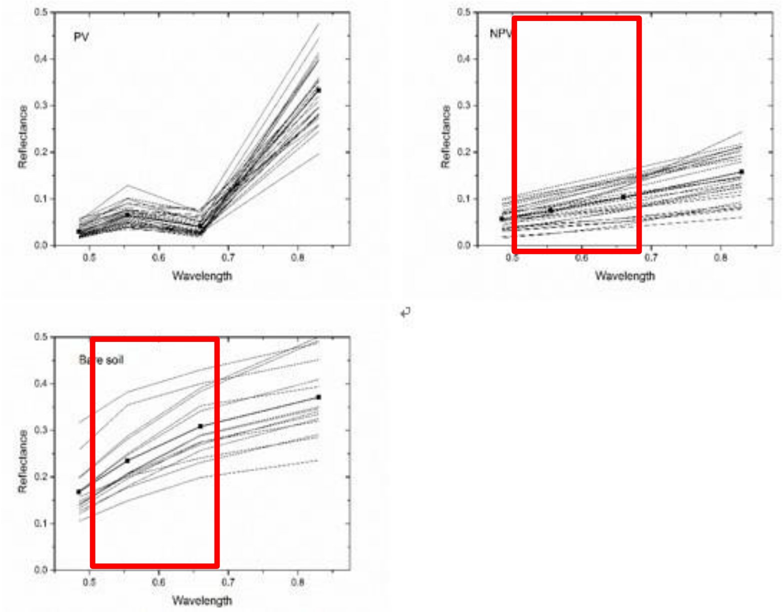

3.1.4 Results

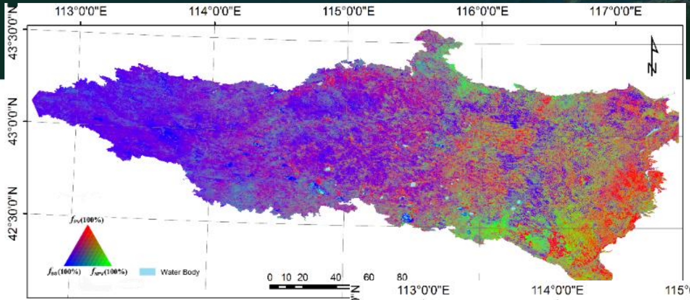

Traditional SMA

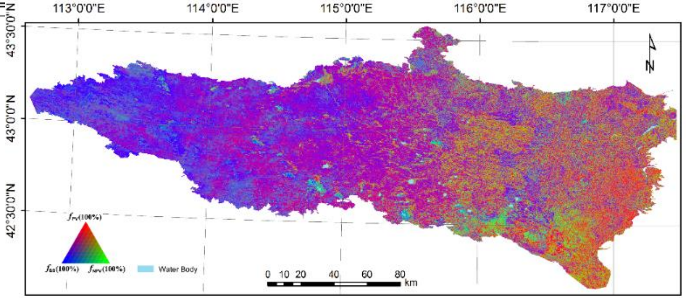

MESMA

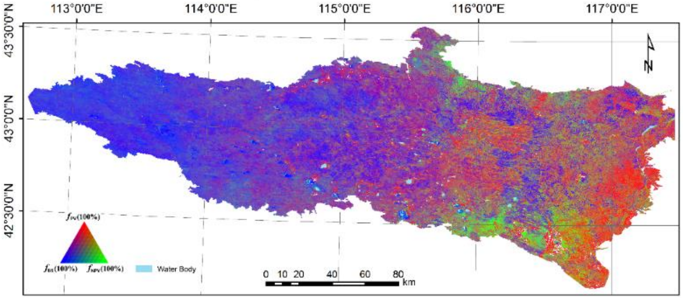

AutoMCU

Comparisons among different methods

- AutoMCU performs best for f_{pv}, f_{npv} estimation compared to SMA and MESMA, with R^2 of 0.49, and RMSE of 0.17 and 0.09 for for f_{pv}, f_{npv}. The problems of f_{npv} overestimation and f_{pv} underestimation in SMA and MESMA were resolved effectively.
- MESMA would produce higher error in f_{npv} estimation , while improve the accuracy of f_{pv} estimation, compared to SMA.

Unmixing apprpach	R^2			RMSE		
	PV	NPV	BS	PV	NPV	BS
AutoMCU	0.49*	0.49*	0. 48*	0.17	0.09	0. 20
MESMA	0.48*	0.11	0. 15	0.21	0.24	0. 21
SMA	0.47*	0.41*	0. 47*	0.27	0. 20	0. 17

Cross-multispectral sensors comparison

- For f_{pv} estimation, this study showed relative lower accuracy, the lowest RMSE acquired by AutoMCU was 17%, the numbers based on the range from 7% to 14.7%.
- For f_{npv} estimation, this study showed some advantage , the lowest RMSE acquired by AutoMCU was 9%, compared to the previous study's 12-20.5%.

#	*Reference*	*Source data*	*Study region and area*	*Study perional*	*Approach*	*Validation points*	*RMSE of f_{pv}*	*RMSE of f_{npv}*
1	Guerschman et al. (2012)	MODIS NDVI and the ratio of MODIS bands 7 and 6	Australia ~7.7 ×10^6 km^2	2000-2010	SMA	*567*	*14.7%*	*20.5%*
2	Okin et al.(2013)	MODIS	Rain-fed cropping region of South Australia. ~150 km^2	Apr, Jul and Oct 2010	SMA, MESMA	*27*	*7-23%*	*12-29%*
3	Guerschman et al. (2015)	Landsat and MODIS	Australia ~7.7 ×10^6 km^2	2000-2013	SMA	*1171*	*11.2-11.9%*	*16.2-17.4%*
4	Current study	GF-1 WFV	Otindag sandy land of North China. ~3.0×10^4 km^2	Peak growing season, 2014	SMA, MESMA and AutoMCU	*121*	*17-27%*	*9-24%*

3.1.5 Conclusions

1. Despite of the spectral similarity of NPV and bare soil, there do exist some differences at GF-1 WFV bands in Otindag sandy land, which could be utilized.
2. Due to the complex ecosystem structure of the Otinday sandy land, the PV, NPV and bare soil endmember libraries showed great intra-variability.
3. SMA should be used with more cautious in quantitative study. MESMA can not be assumed performing always better than SMA, due to the coupling of the NPV and bare soil EMs. AutoMCU was proved effective for dealing with the EM variability .
4. GF-1 WFV data was proved to be capable for fpv and fnpv estimation in Otinday sandy land, although lacking the important SWIR bands. With GF-1 WFV's unique advantage of high spatial resolution, wide coverage and high revisit frequency, great potential existed for relevant analysis in the future.

Contents

3 Extraction of Desertification Information from Remote Sensing data

3.2 Sandy Land detection by Spectral Mixture Analysis

- Vegetation covers the soil information to a great extent, it is difficult to detect the sandy Land or desertification based on remote sensing image;

- Transitional sandy land is difficult to extract, its boundary is hard to define exactly, and efficiency of qualitative classification is relatively lower;

- Against the problems above, Spectral Mixture Analysis (SMA) was applied to solve vegetation cover and transitional sandy land detection.

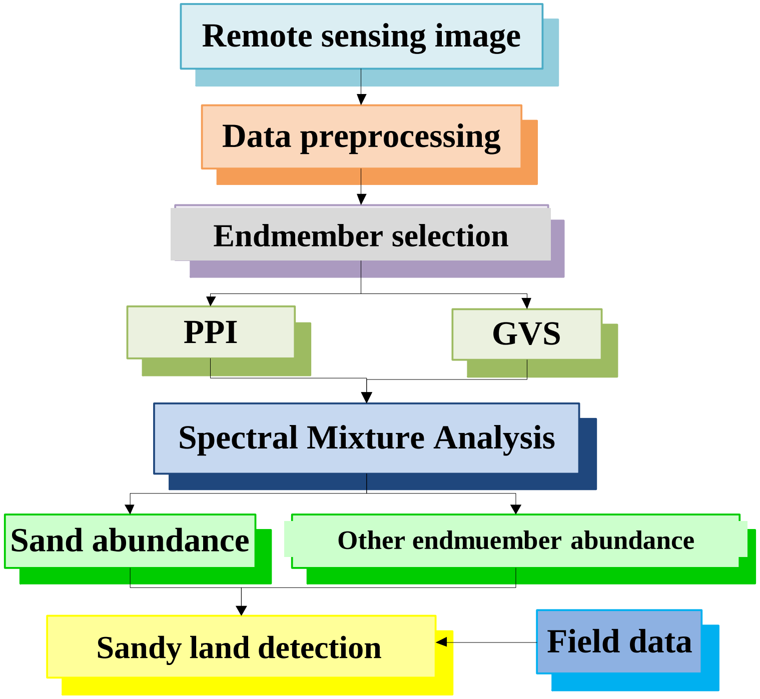

Flowchart of technique route

3.2.1 Test site and data

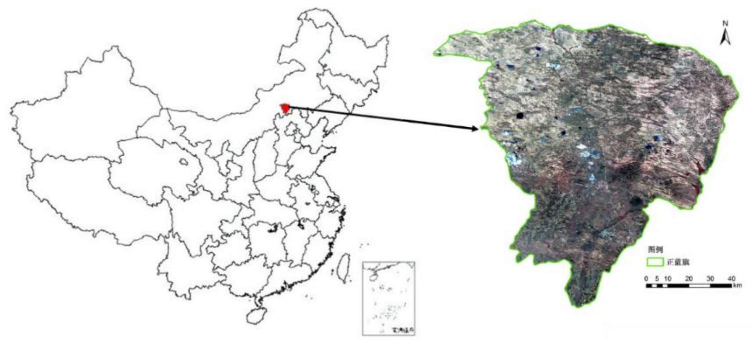

- Image type: GF-1
- Spatial resolution : 16m
- Imaging time: 2014.04.27

3.2.2 Endmember selection method

- Pure Pixel Index (PPI)
- Geometric vertex of scatterplot (GVS)

GVS

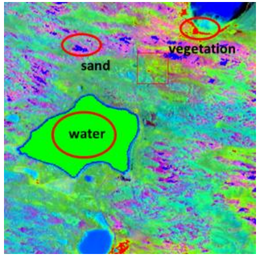

Minimum Noise Fraction,MNF

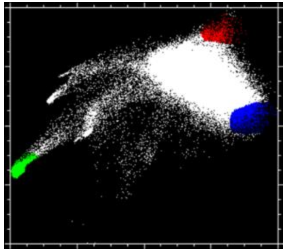

2D-splattering

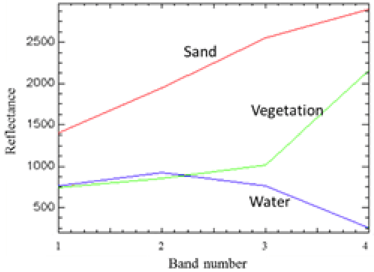

Endmember spectral plot

PPI

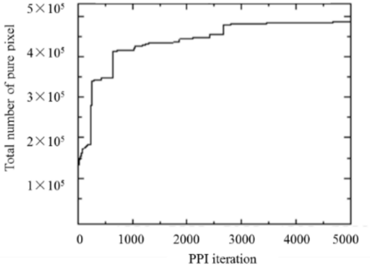

PPI iteration

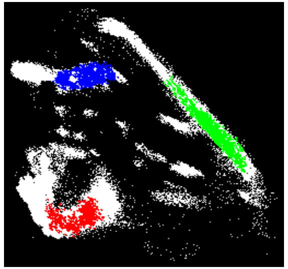

3D-splattering

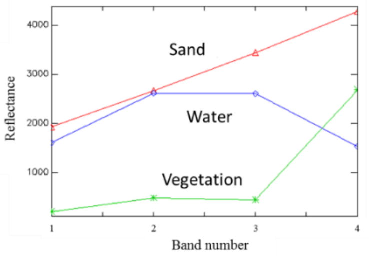

Endmember spectral plot

- PPI was better than GVS, the endmember spectral was more classic and suitable

Endmember number

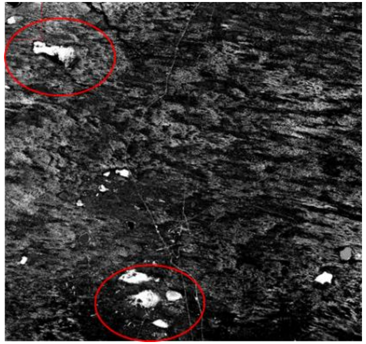

N=3

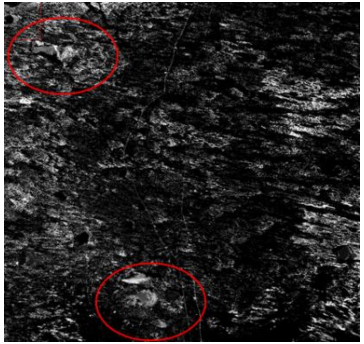

N=6

❶ if the number was greater than 6, it was prone to generate noise and error;

❷ if the number was less than 5, the mixed pixel couldn't be decomposed effectively;

❸ the endmember number was 5 or 6 in this study was more suitable, the decomposition result would be more accurate in the degraded land detection.

Endmember type

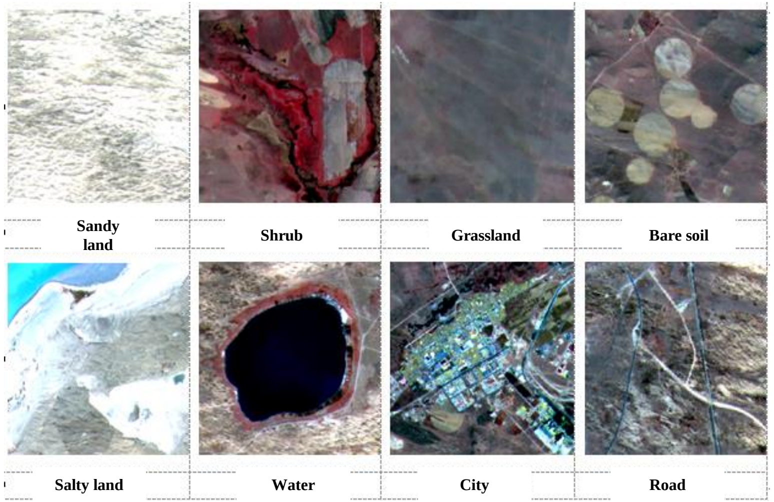

Pictures of several typical lands in GF-1 image during the ungrowing season

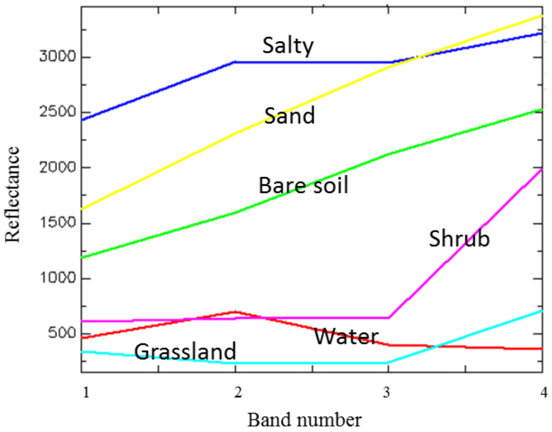

Endmembers spectral plots

Spectral Mixture Analysis

- Linear Spectral Unmixing (LSU) $D_{Ni} = \sum_{j=1}^{p} m_{ij}\alpha_j + e_i$ $\alpha_1 + \alpha_2 + \ldots + \alpha_j = 1$

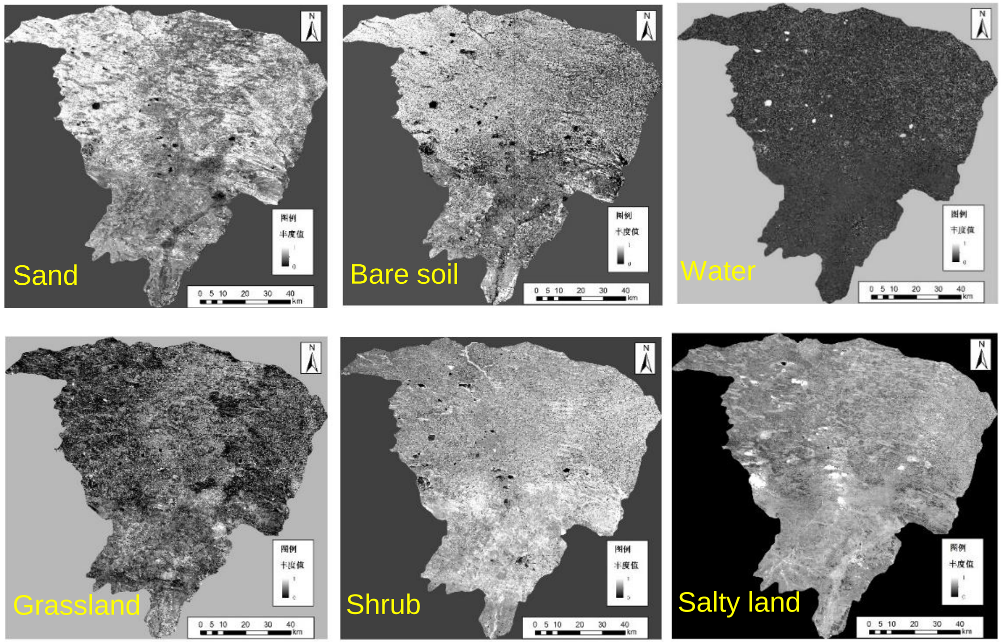

Abundance distribution of different endmember based on PPI

3.2.3 Sandy Land detection

- ❶ If sand abundance accounted for more than 50% in the remaining endmember abundance except for vegetation, or less than 50% but it was the maximum , the pixels would be determined as sandy land.
- ❷ The total accuracy was 86.42%, the transitional sandy land with high vegetation coverage could be also extracted accurately and effectively.

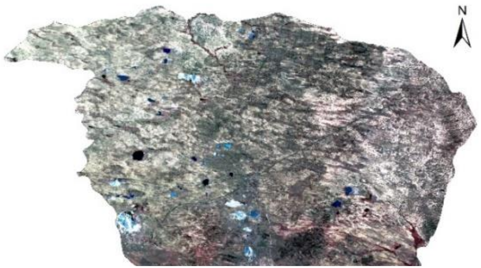

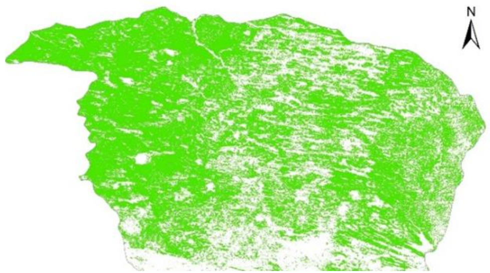

Projects	Total number	Sandy land	Unsandy land
Sample number	162	81	81
Correct number	140	68	72
Accuracy	86.42%	83.95%	88.89%

Contents

Estimating Above Ground Biomass of Otindag Sandy land by Using Chinese and European Earth Observation data and Machine Learning

CONTENTS

3.3.1 Introduction

- **Land degradation in dryland has become one of the major environmental problems.**
- **Land degradation indicators identification is one of the most important tasks in achieving of UN 's sustainable development goals（SDGs） 15: Life on Land and 2: Zero Hunger.**
- **Vegetation above ground biomass (AGB) could reflect the land productive capacity well.**
- **Refined estimation of AGB in dryland has a great scientific significance to the dryland ecosystem management and desertification assessment and monitoring.**

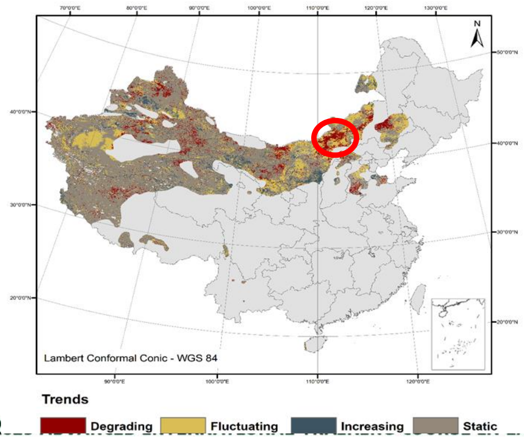

Dragon 4 cooperation research results (Project ID:32396)

Land condition trends for PEDC during 2003-2011 based on MERIS data

UN SDGs (2016-2030)

3.3.1 Introduction

Challenges for AGB estimation in dryland

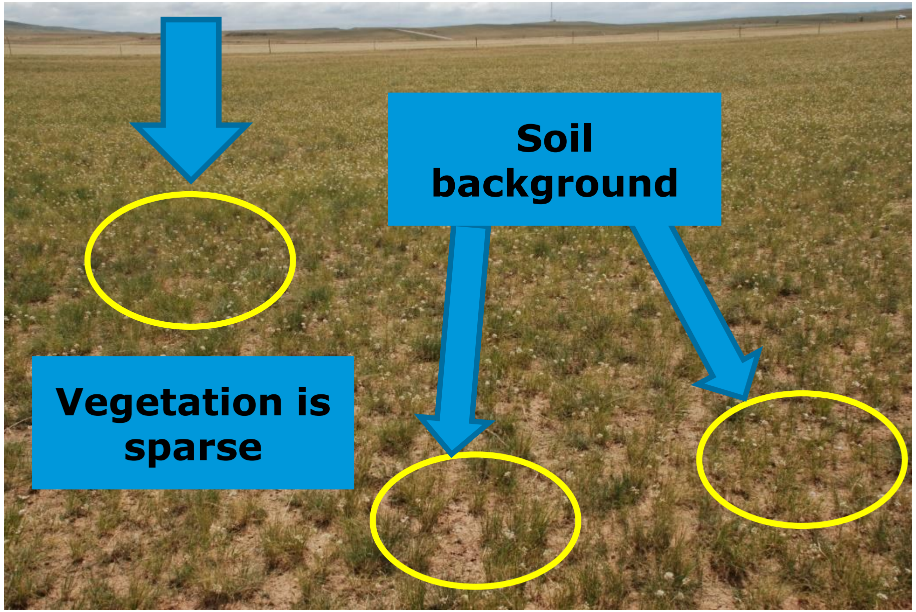

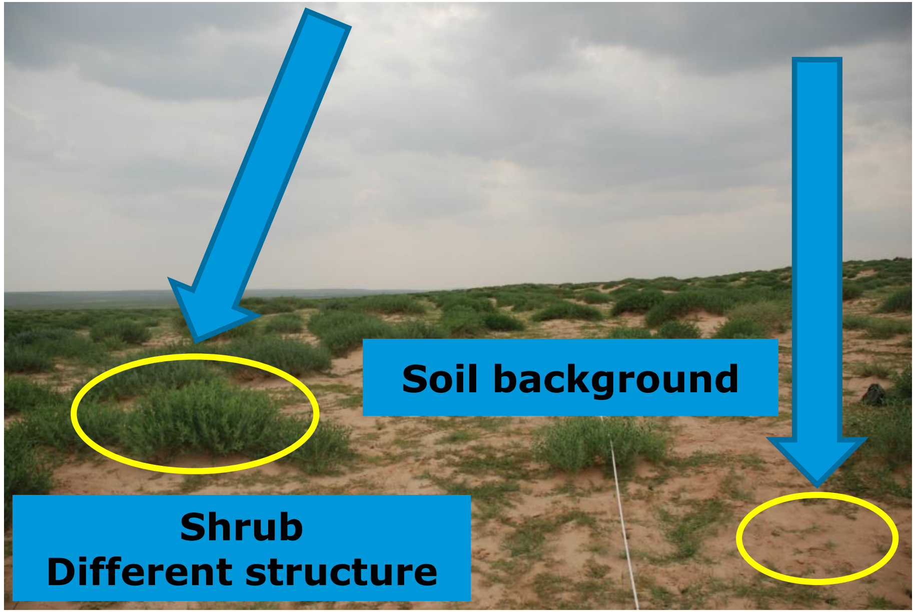

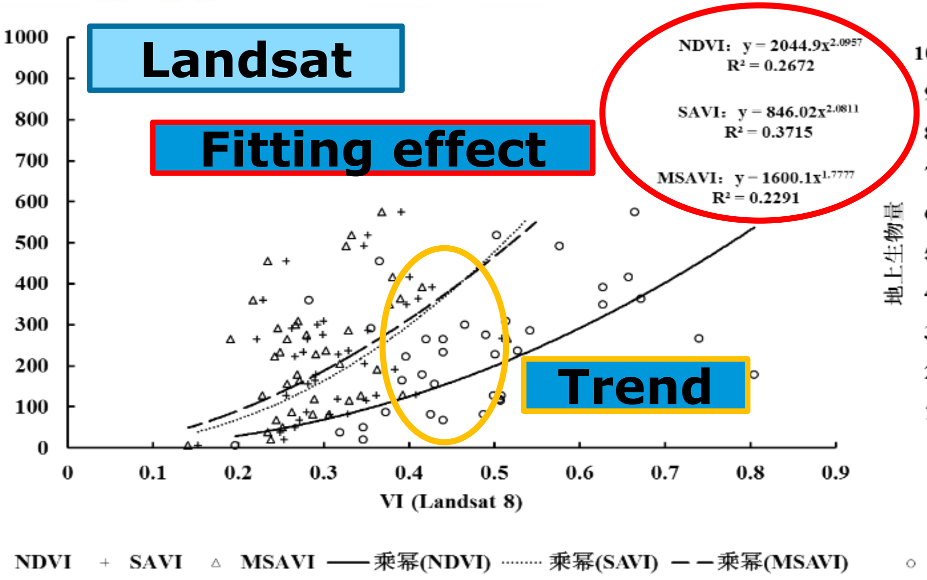

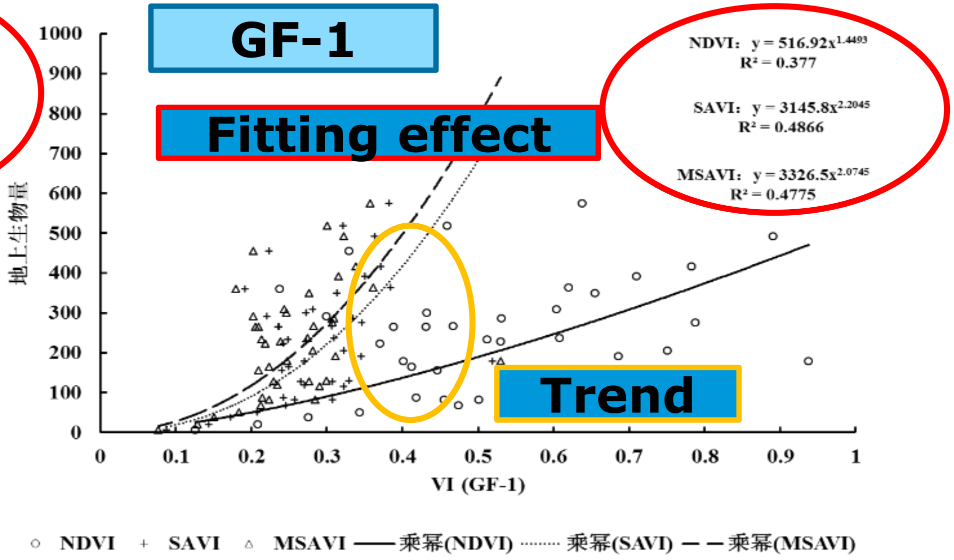

NDVI、SAVI、MSAVI and regression method

Method: parametric
Data: VIs

Method: nonparametric
Data: Band information/VIs/Texture

Wavelengths and Bandwidths of the three Spatial Resolutions of the MSI instruments Sentinel-2 Product

Spatial Resolution (m)	Band Number	Central Wavelength (nm)	Bandwidth (nm)
10	2	490	65
	3	560	35
	4	665	30
	8	842	115
20	5	705	15
	6	740	15
	7	783	20
	8a	865	20
	11	1610	90
	12	2190	180
60	1	443	20
	9	945	20
	10	1380	30

Technical parameters of GF-1 WFV

Parameters	16m WFV
Spectral rang（μm）	B1:0.45-0.52 B2:0.52-0.59 B3:0.63-0.69 B4:0.77-0.89
Spatial resolution（m）	16
Swath width（km）	4 Cameras spliced width of 800
Coverage period	4days

- ✓ **To develop a useful method for sparse vegetation aboveground biomass inversion in dryland by integrating remote sensing information and field survey data.**
- ✓ **To compare the application ability of EO data from Chinese and European side in the extraction of sparse vegetation aboveground biomass in dryland.**

CONTENTS

3.3.2 STUDY AREA AND DATA COLLECTION

3.3.2.1 Study area

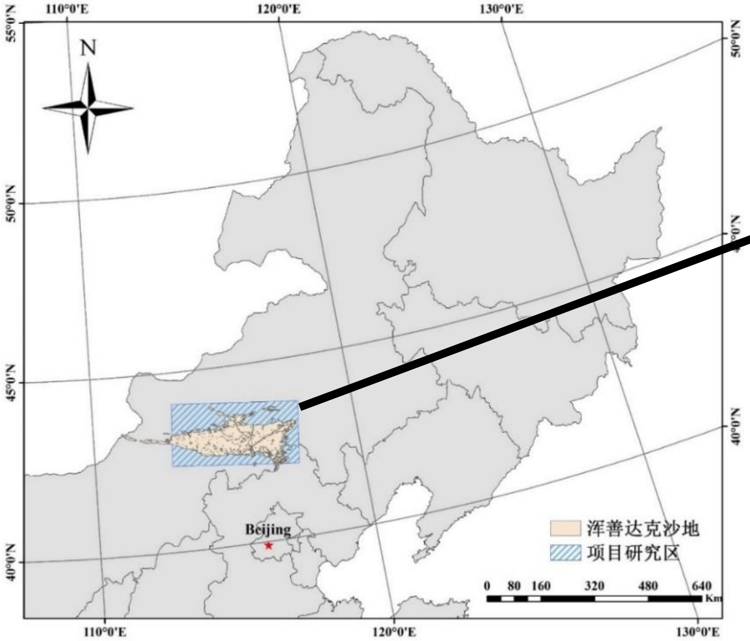

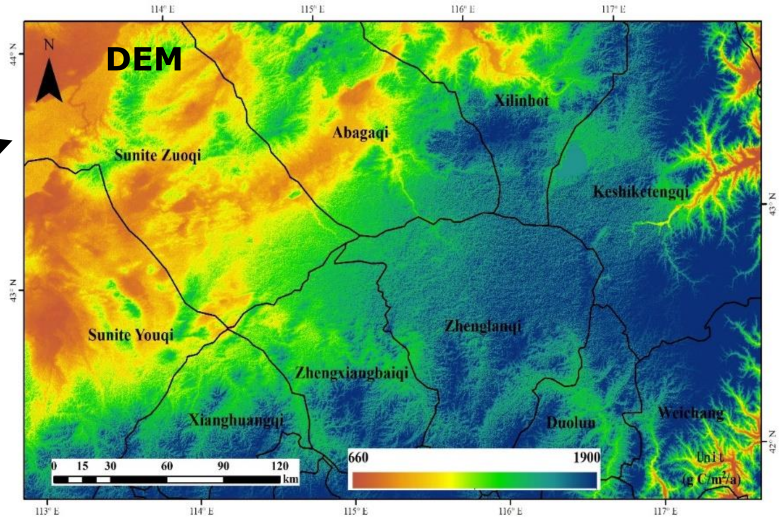

- ✓ Located in **semi-humid** zone.
- ✓ Covering typical **grassland and sandyland vegetation**.
- ✓ **OSLAIS, Key part of the Beijing-Tianjin Sand Source Region.**

3.3.2.2 EO data

□ EO data Sentinel-2 Covering growing season (July-August)

Table of sentinel-2 data acquisition

Imaging time	Scenes	Month/date	Cloud coverage and quality
2015	2	10^{th} , August	Clouds<1%, Good quality
2016	34	Jul- Aug	Good quality
2017	55	Jul- Aug	Clouds<1%, Good quality

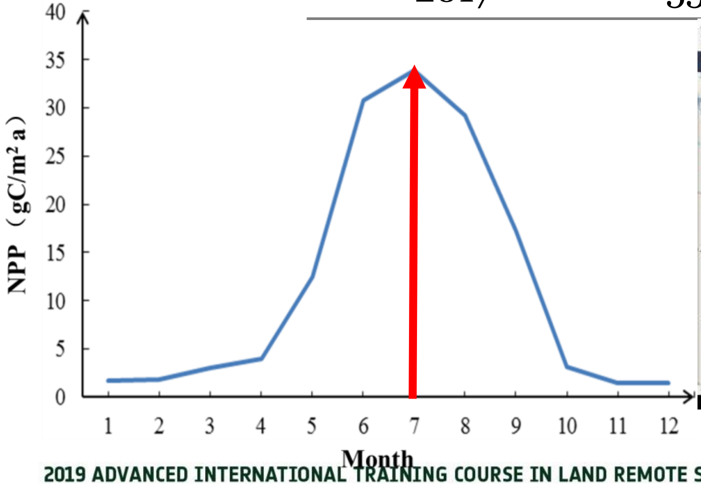

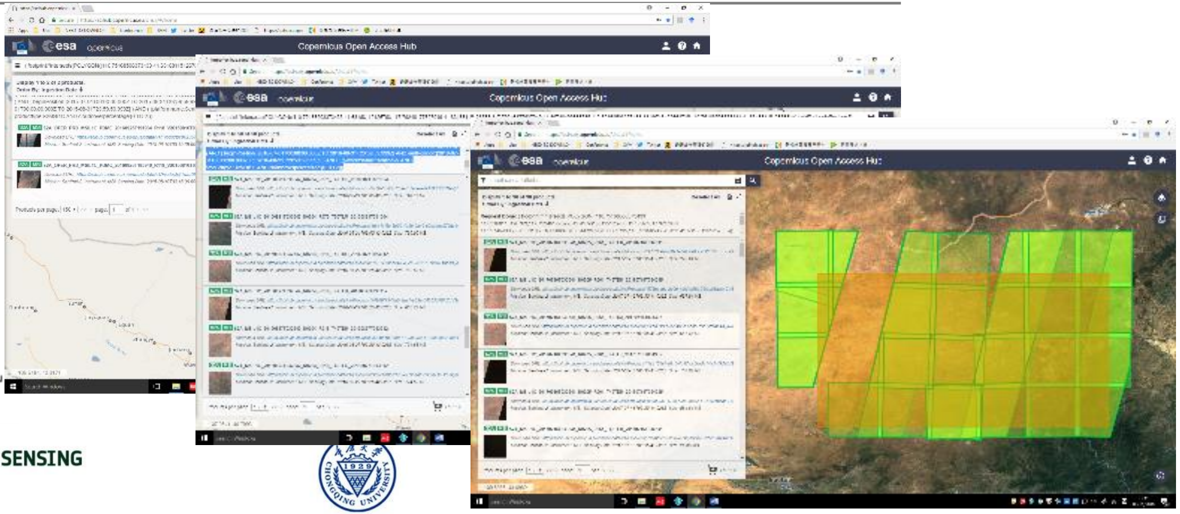

◻ EO data GF-1

Table of GF-1 WFV data acquisition

Year	Jul	Aug	Sep	Total	Cloud coverage and quality	Coverage
2015	-	-	6*	6	Clouds<1%,Good quality	100%
2016	-	6	-	6	Clouds<1%,Good quality	100%
2017	5	-	-	5	Clouds<1%,Good quality	100%

* Single scene image width 200km.

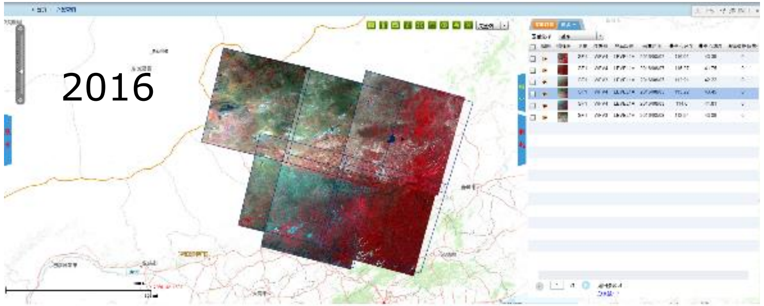

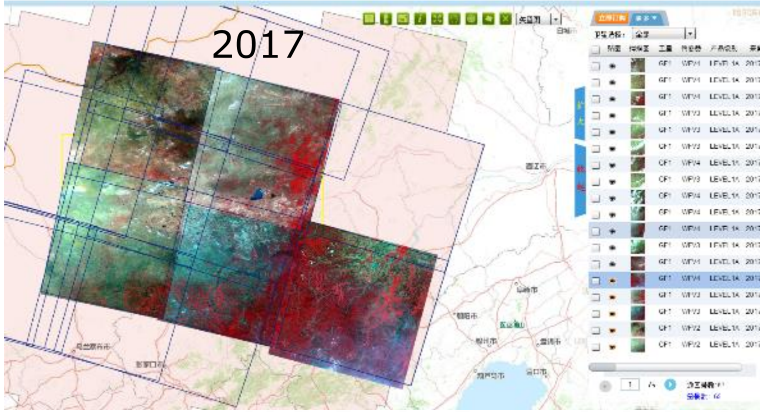

3.3.2.3 Field survey data

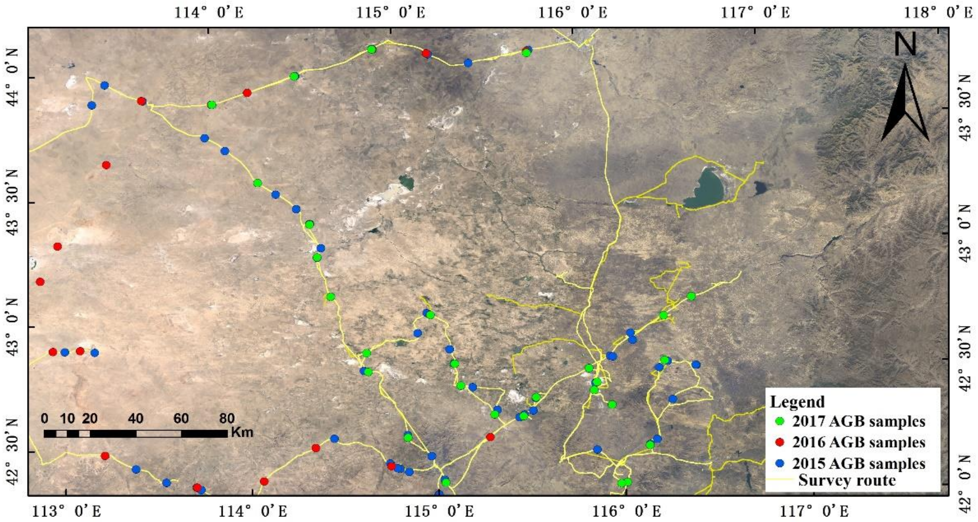

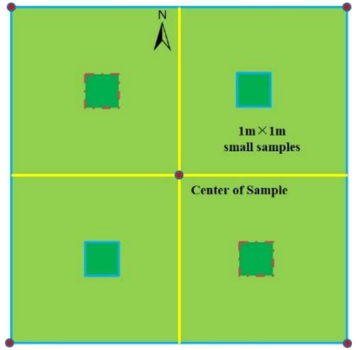

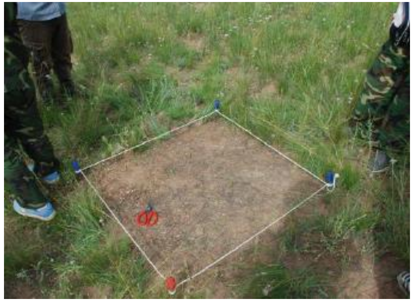

Sampling sites implantation and AGB evaluation by the "Harvest method"

Samples using for AGB estimation –GF-1 data

Year	July-August	Grassland	Mixing(shrub + grass)
2016	30	24	6
2017	40	31	9
Total	70	45	15

Samples using for AGB estimation - S2 data

Year	July-August	Grassland	Mixing(shrub + grass)
2015	52	37	15
2016	15	11	4
2017	31	21	10
Total	98	69	29

CONTENTS

3.3.3 EO DATA PROCESSING AND METHODS

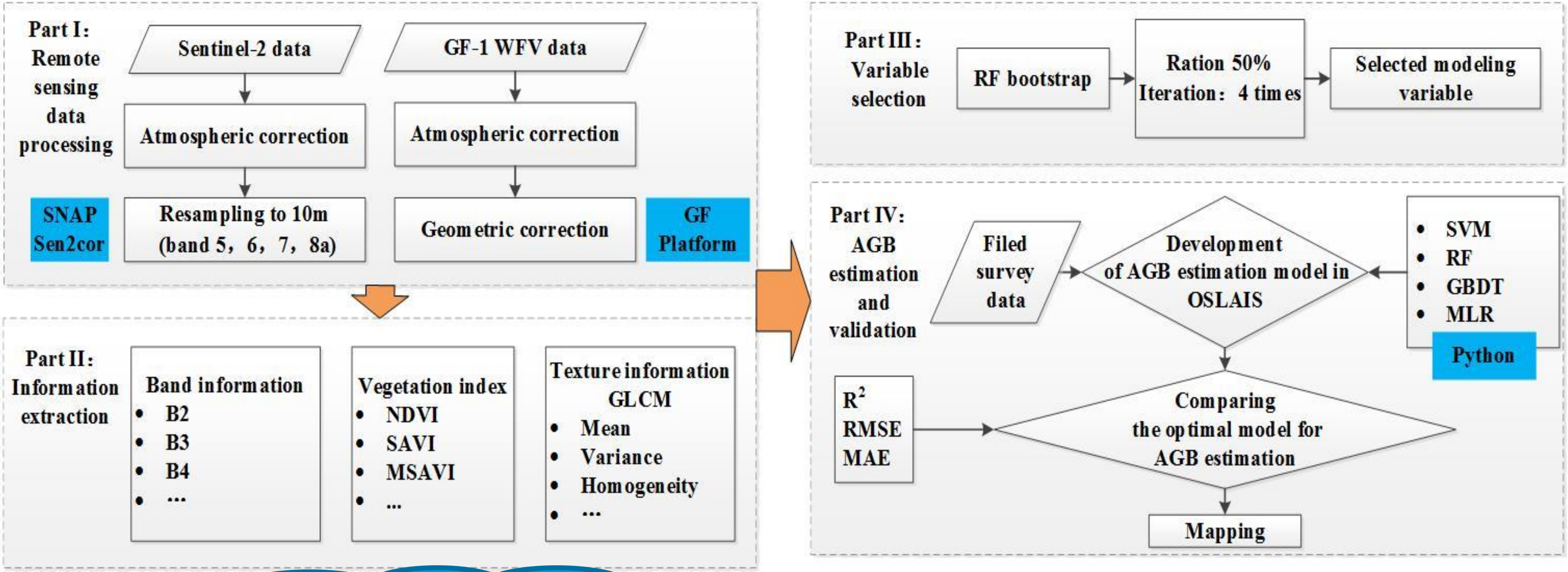

Cloud platform provided through the ESA Network of Resource Initiative

Technical flow chart in this study

3.3.3.1 EO data processing

AC of S2 by using the Sen2cor provided by ESA

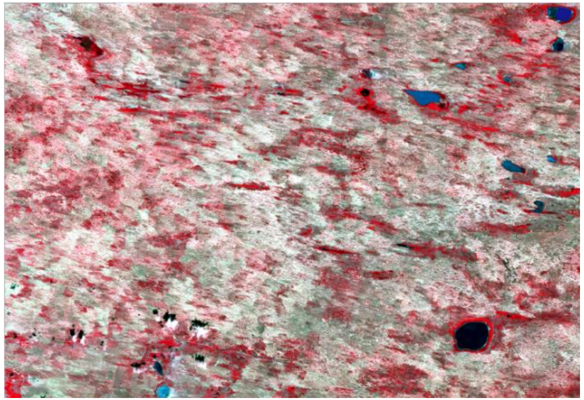

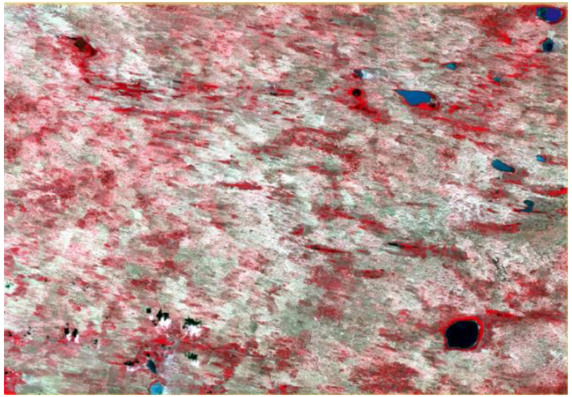

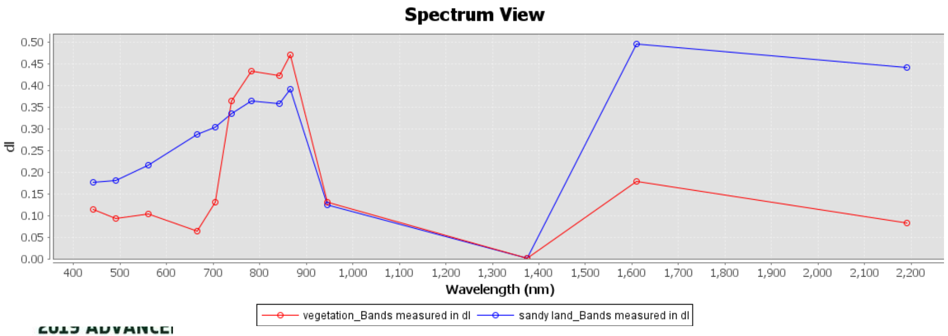

Before Atmospheric correction

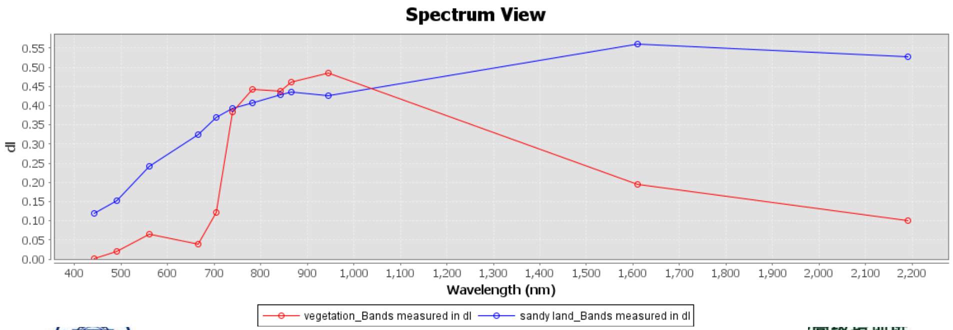

After Atmospheric correction

AC of GF-1 by using the FLAASH algorithm

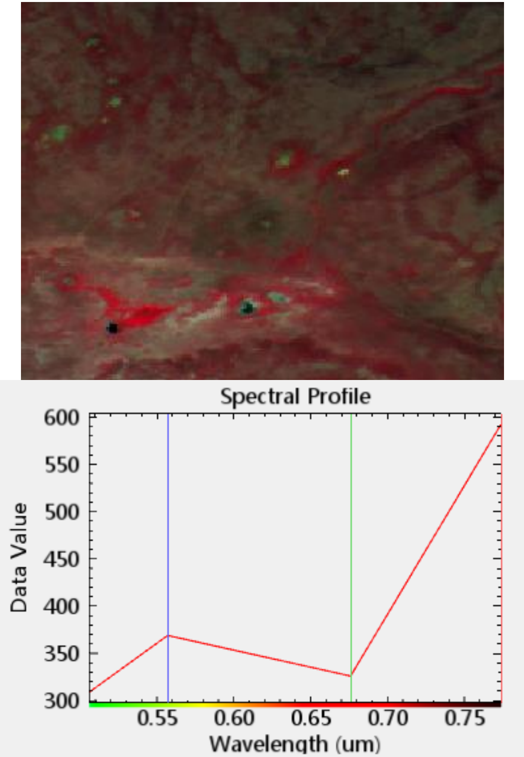

Before Atmospheric correction

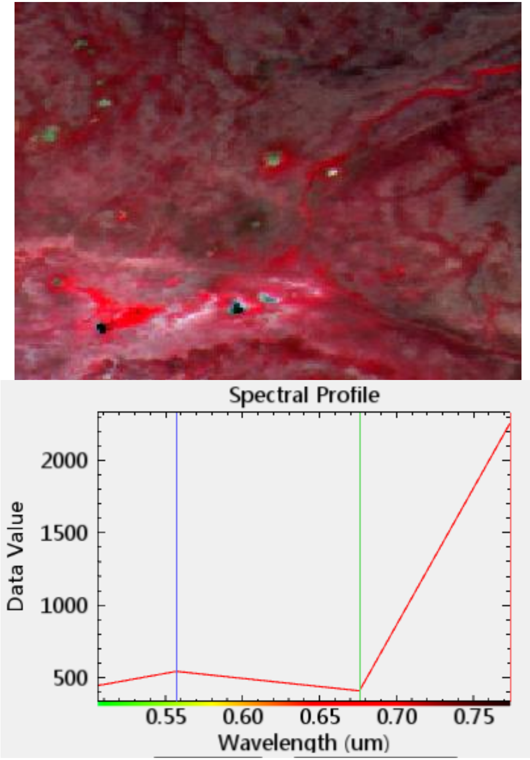

After Atmospheric correction

Geometric correction (GC)
The processing was conducted in ENVI 5.0, and no fewer than 50 evenly distributed control points were selected for each image.

Gaofen forestry demonstration platform for remote sensing applications-CAF

Type	Variable	S2	GF-1	Type	variable	S2	GF-1
Band Reflectance	Blue	√	√	VI	NDVI	√	√
	Green	√	√		SAVI	√	√
	Red	√	√		TSAVI	√	√
	Vegetation-red edge1	√			MSAVI	√	√
	Vegetation-red edge2	√			DVI	√	√
	Vegetation-red edge3	√			RVI	√	√
	NIR	√	√		PVI	√	√
	Narrow NIR	√			GNDVI	√	√
Texture information (GLCM)	Contrast	√	√		NDI45	√	
	Dissimilarity	√	√		MTCI	√	
	Homogeneity	√	√		MCARI	√	
	Angular second moment	√	√		REIP	√	
	Energy	√			S2REP	√	
	Maximum probability	√			IRECI	√	
	Entropy	√	√		PSSRa	√	
	GLCM mean	√	√				
	GLCM Variance	√	√				
	GLCM Correlation	√	√				

3.3.3.2 Information extraction from EO data for AGB estimation

Bands reflectance

Texture information

Vegetation index

S2:103

GF-1:44

Texture information

- **Gray-Level Co-occurrence Matrix (GLCM)**
- **Window size GF-1 :“3×3” and S2 : “5×5”**

SNAP

“Raster-->Image Aanlysis-->Texture Analysis”

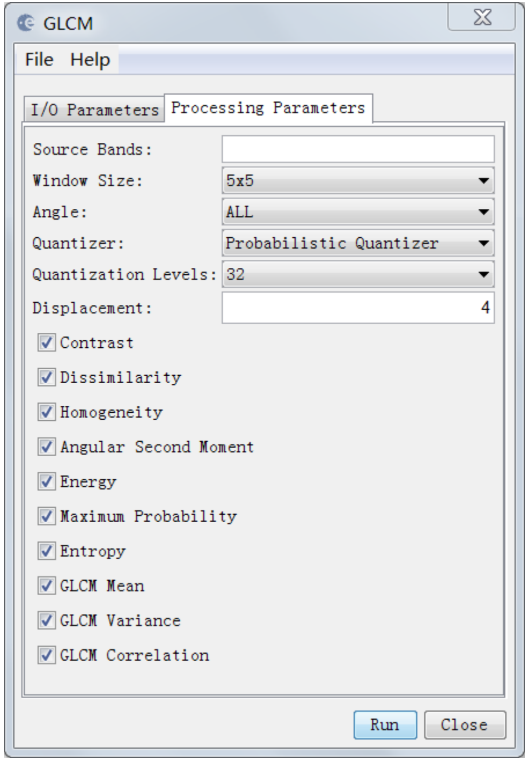

Vegetation index

Equations of the fourteen VIs calculation based on Sentinel-2 image

Not contain red edge band		Contain red edge band	
VI	Equation	VI	Equation
NDVI	(NIR - R)/(NIR + R)	NDI45	$(B_5-B_4)/(B_5+B_4)$
SAVI	((NIR - R)/(NIR + R +L))(1+L) *	MTCI	$(B_6-B_5)/(B_5-B_4)$
TSAVI	$a(NIR-aR-b)/(aNIR+R-ab+c(1+a^2)$ **	MCARI	$[(B_5-B_4)-0.2\times (B_5-B_3)] \times (B_5-B_4)$
MSAVI	$((2NIR+1-((2NIR+1)^2-8(NIR-R))$^0.5)/2	REIP	$700+40\times[(B_4+B_7/2-B_5)/(B_6-B_5)]$
DVI	NIR - R	S2REP	$705+35\times[(B_4+B_7/2-B_5)/(B_6-B_5)]$
RVI	NIR / R	IRECI	$(B_7-B_4)/(B_5/B_6)$
PVI	sin(a) ×B8-cos(a) × R	PSSRa	B_7/B_4
GDVI	(NIR -G)/(NIR +G)		

Note: NIR= Near infrared band reflectance; R= Red band reflectance; G= Green band reflectance; *L=0.5 ; **a=0.5, b=0.5, c=0.08; Bi is the i band reflectance of sentinel-2 image.

Vegetation index

SNAP

"Opitical-->Thematic Land processing -->Vegetation Radiometric Indices"

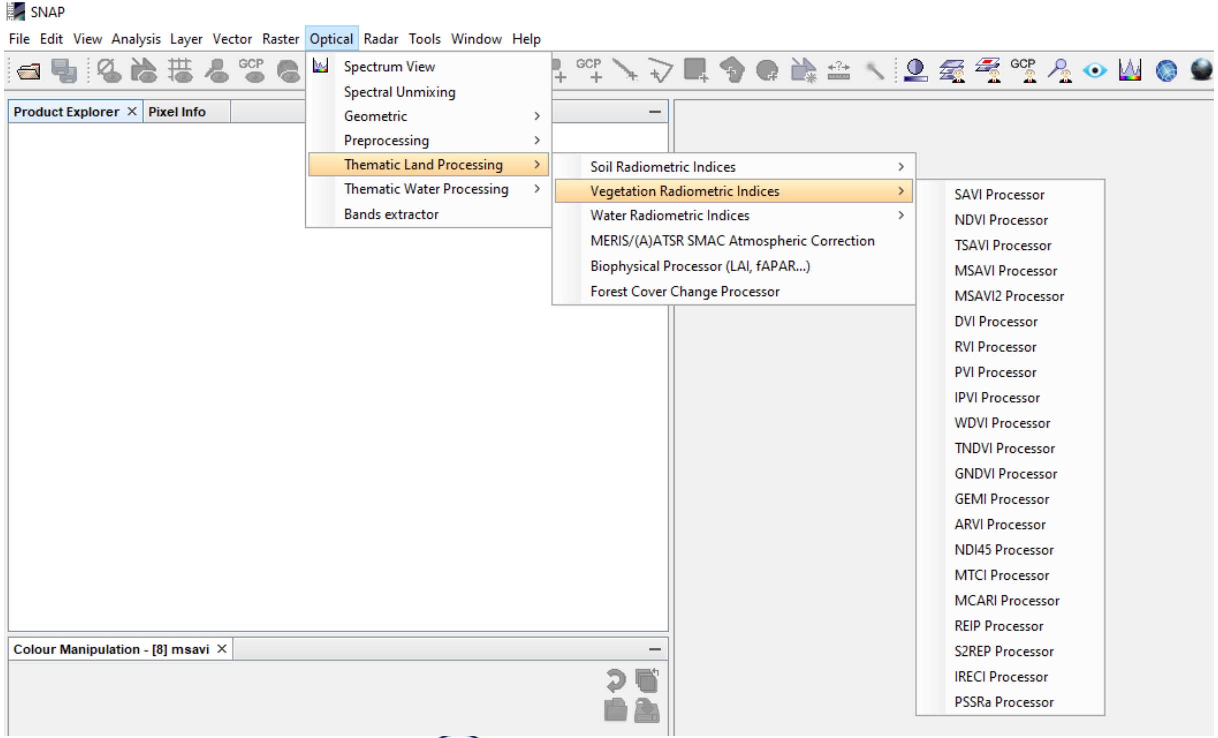

Values extraction from the EO data

Window size

- **GF-1 :“3×3” and S2 : “5×5”** ***VI BR***
- **GF-1 :“1×1” and S2 : “1×1”** ***TI***

SNAP

“Raster-->Export--> Extract Pixel Values”

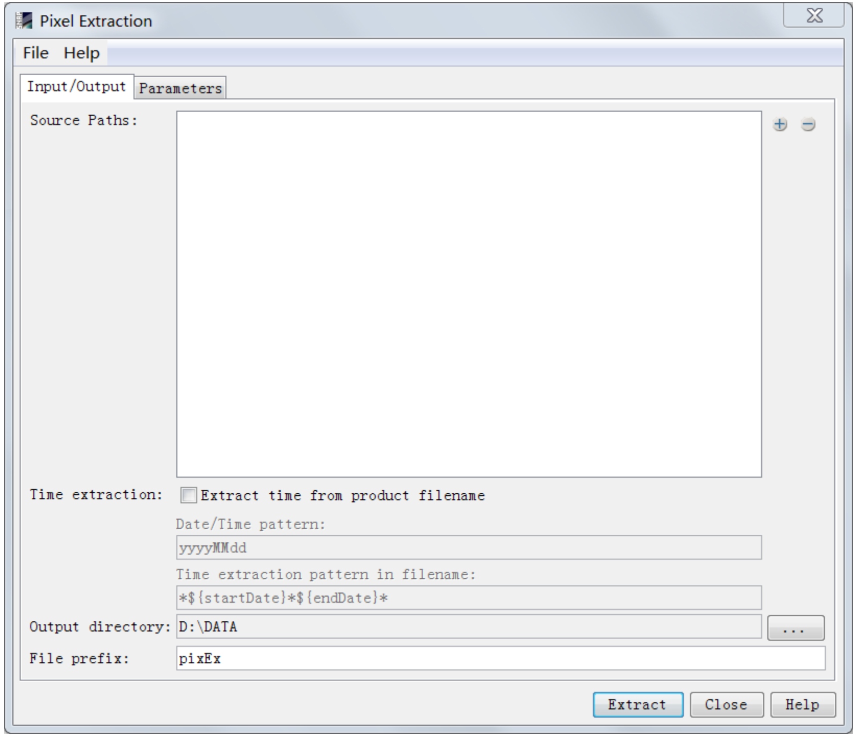

3.3.3.3 Variable selection

- *Python package (vers. 3.6.8)*
- *RF bootstrap method and Multiple times iteration*
- *Half-Half in every iteration*
- *4 times iteration*

3.3.3.4 AGB estimation and validation

Empirical modeling approaches

- *Simple linear regression*
- *Random forest (RF)*
- *Gradient boosting Decision Tree (GBDT)*
- *Support Vector Machine (SVM)*
- *Multi-Linear Regression (MLR)*

Validation

- *5-fold cross validation*
- *Training (80%) and testing (20%)*
- *R^2 , RMSE and MAE*

CONTENTS

3.3.4. RESULTS AND ANALYSIS

3.3.4.1 Importance of the variables for the AGB estimation

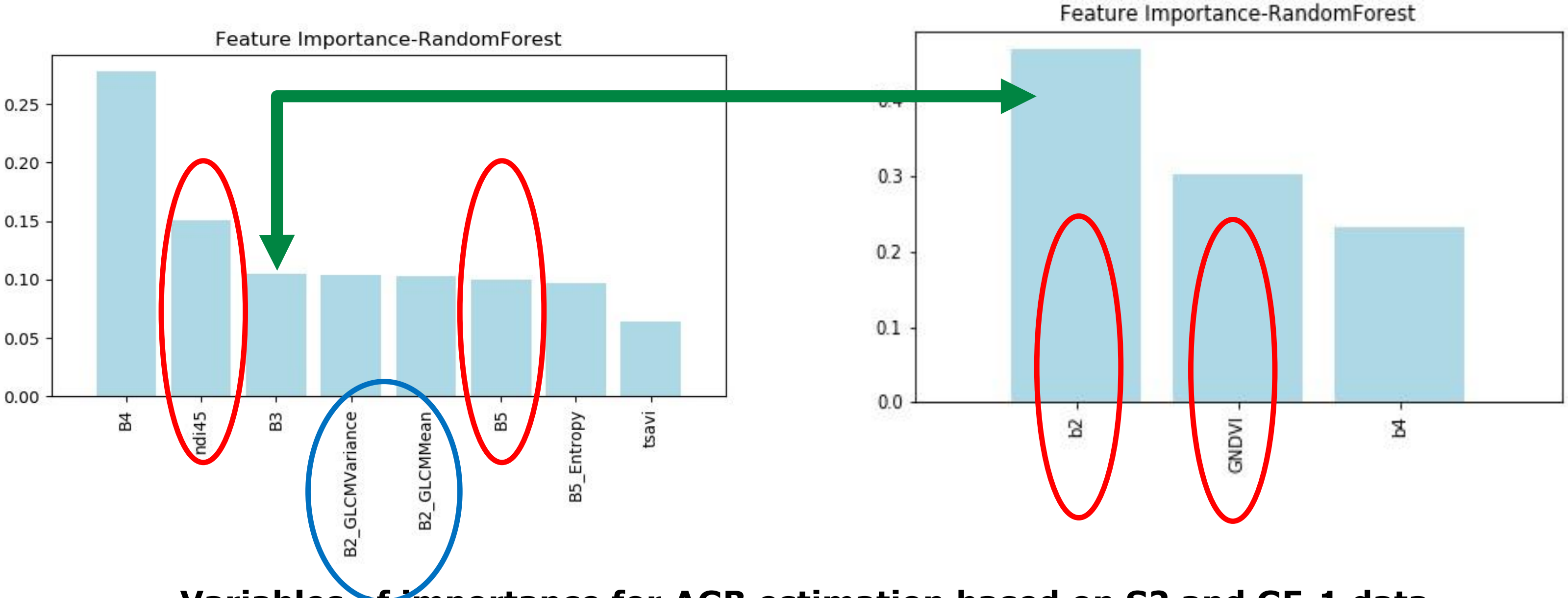

Variables of importance for AGB estimation based on S2 and GF-1 data

3.3.4.2 Construction of AGB estimation models and validation

Accuracy assessment of the AGB estimation models using 5-fold cross validation method based on S2 images.

Approach	R^2	RMSE	MAE	Models
SVM	0.71	23.76	19.84	Non-linear
RF	0.57	28.97	22.17	Non-linear
GBDT	0.55	29.91	22.00	Non-linear
MLR*	0.67	25.51	19.59	Linear

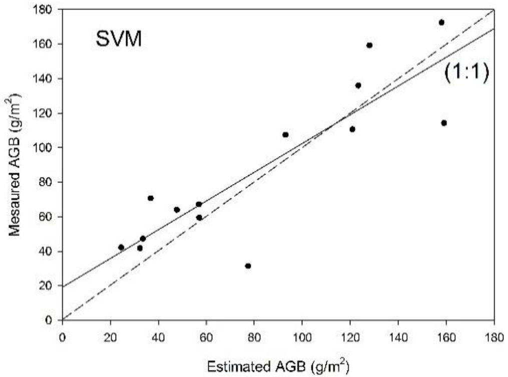

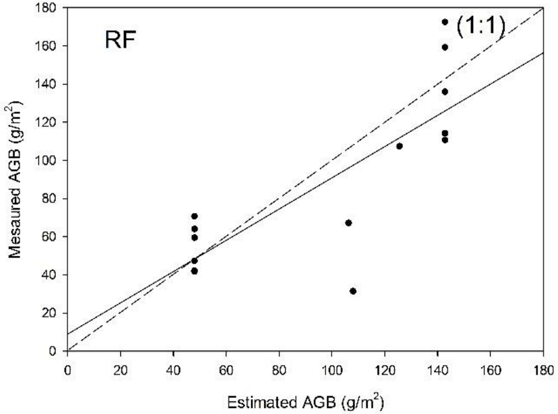

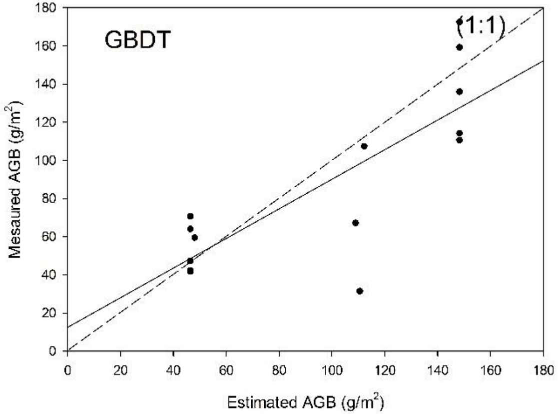

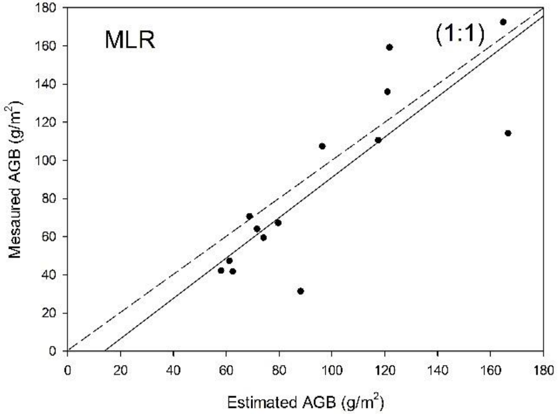

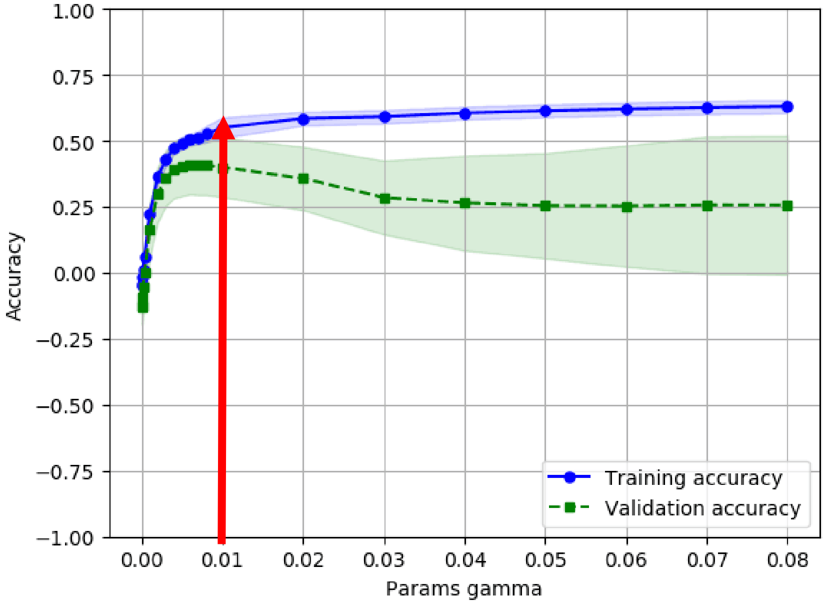

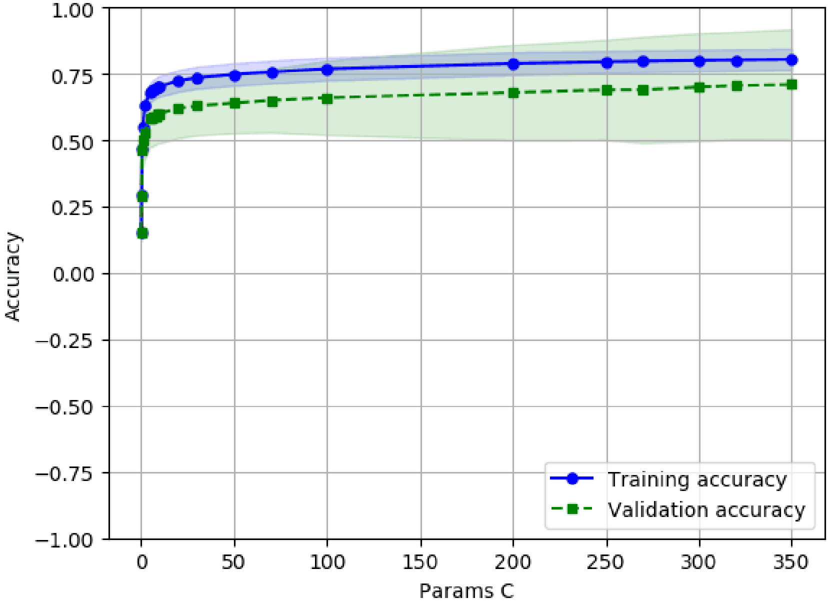

Kernel functions （RBF）， gama and penalty factor C

Accuracy curve of training and validation corresponding the variation of the two key parameters in SVM model

Accuracy assessment of the AGB estimation models using 5-fold cross validation method based on GF-1 WFV images.

Approach	R^2	RMSE	MAE	Models
SVM	0.52	43.15	36.13	Non-linear
RF	0.58	40.25	31.04	Non-linear
GBDT	0.54	42.10	31.56	Non-linear
MLR	0.43	46.96	36.89	Linear

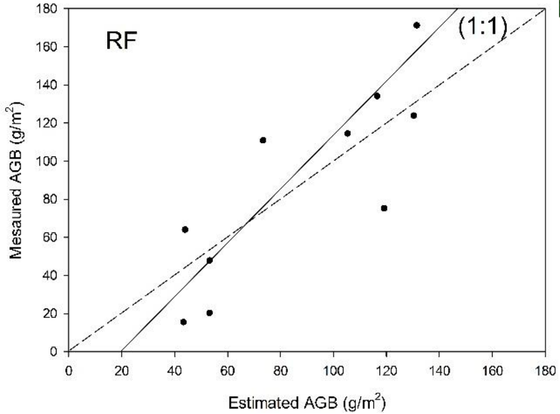

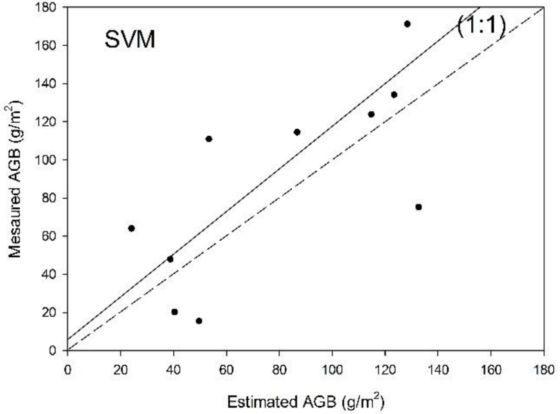

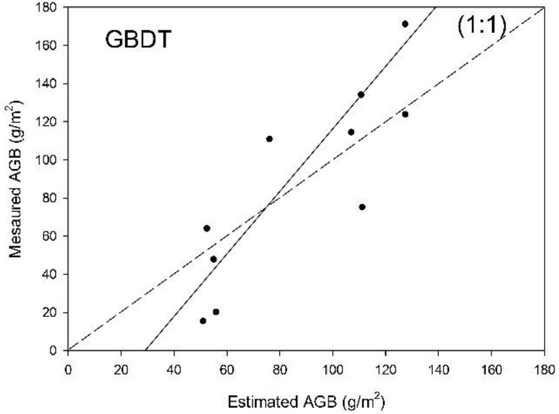

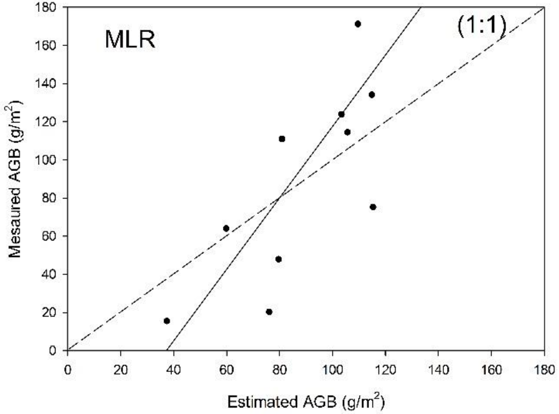

3.3.4.3 Distribution of AGB in Otingdag sandyland

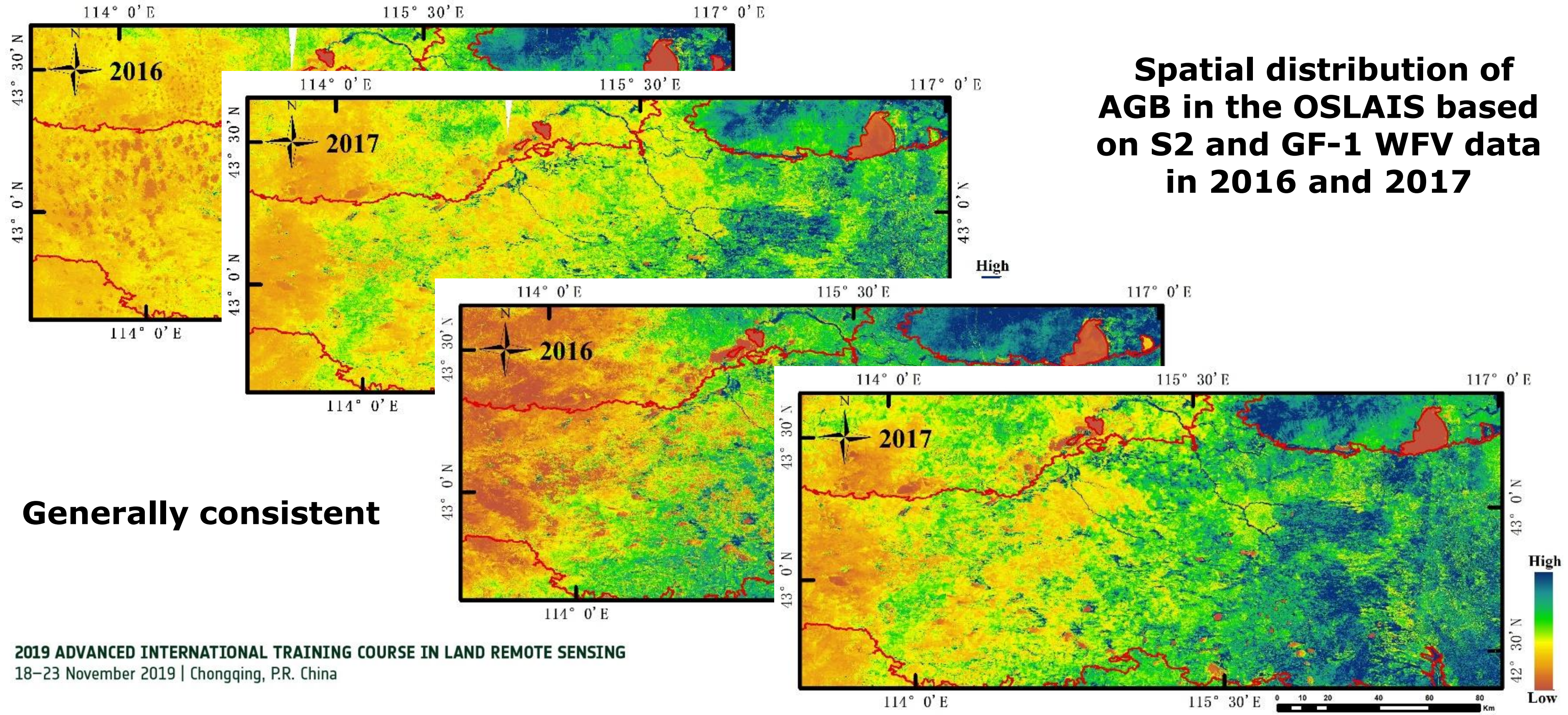

Spatial distribution of AGB in the OSLAIS based on S2 and GF-1 WFV data in 2016 and 2017

Generally consistent

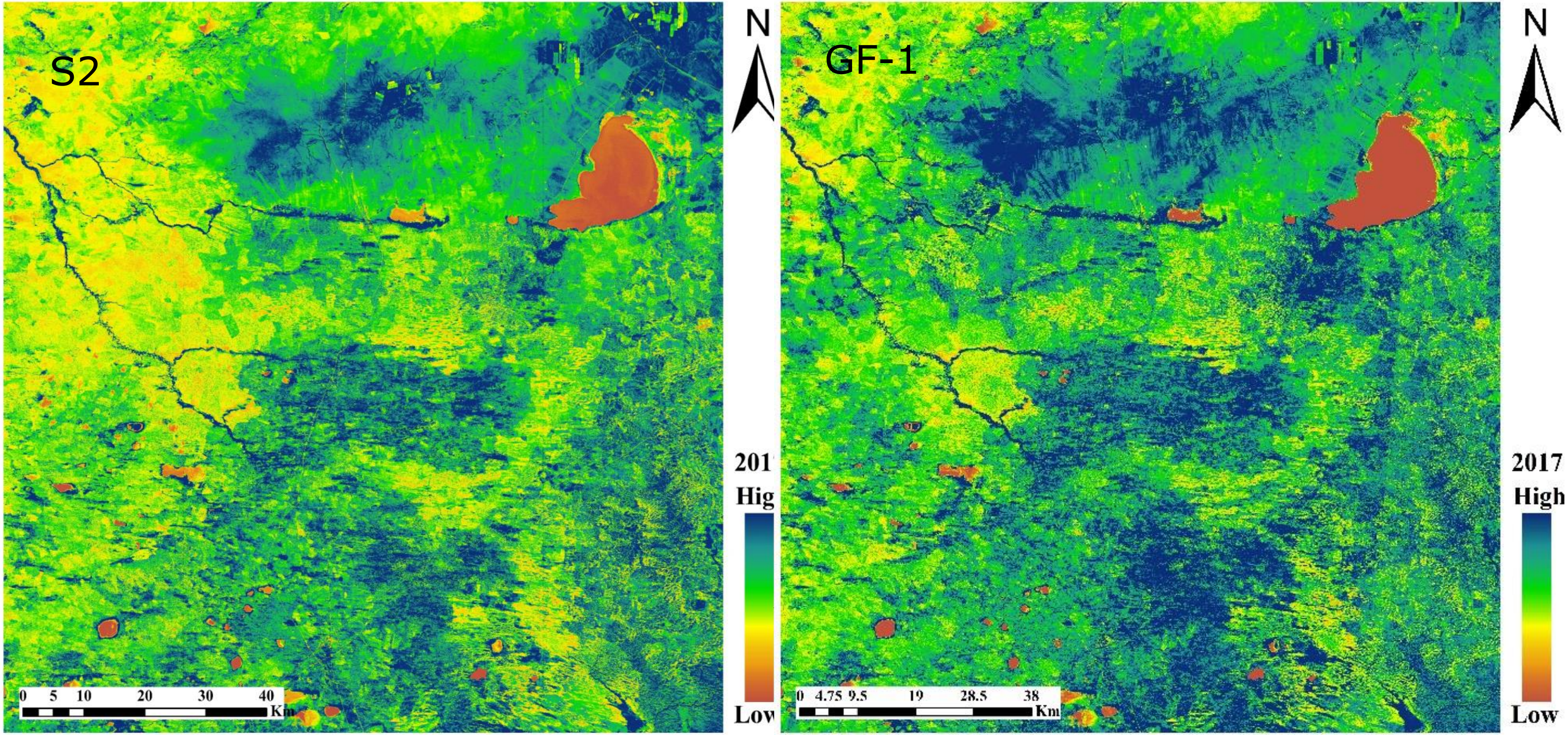
S2
N
201
Hig
Low
0 5 10 20 30 40
Km
GF-1
N
2017
High
Low
0 4.75 9.5 19 28.5 38
Km

3.3.4.4 Compared with the VI-based method

Equations of the fifteen VIs calculation based on Sentinel-2 and GF -1 image

VI	Model Sentinel-2	R^2	Model GF-1	R^2
DVI	$y = 1301\ x^{1.2583}$	0.2557	$y = 724.88\ x + 15.62$	0.1342
SAVI	$y = 600.07\ x^{1.1093}$	0.3187	$y = 91.38 \ln(x) + 253.56$	0.2516
TSAVI	$y = 67.692\ e^{-0.271\ x}$	0.1048	$y = 0.1401x + 95.20$	0.1016
MSAVI	$y = 722.94\ x^{1.1449}$	0.3067	$y = 498.68\ x + 12.91$	0.2207
PVI	$y = 2012.2\ x^{1.2583}$	0.2557	$y = 955.69\ x + 101.47$	0.3100
RVI	$y = 48.513\ x^{1.0387}$	0.2062	$y = 76.539 \ln(x) + 46.638$	0.2223
NDVI	$y = 317.94\ x^{0.9024}$	0.3232	$y = 290.48\ x^{1.0206}$	0.3028
GNDVI	$y = 244.58\ x^{0.9247}$	0.2330	$y = 480.4\ x^{1.9815}$	0.3146

VI	Model Sentinel-2	R^2
NDI45	$y = 555.12\ x^{0.8052}$	0.2116
MTCI	$y = 36.419\ e^{0.7078\ x}$	0.2895
MCARI	$y = 412.95\ x^{0.4285}$	0.0809
REIP	$y = 1825.3e^{-0.004\ x}$	0.0027
S2REP	$y = 1.089\ x^{-651.91}$	0.0224
IRECI	$y = 323.04\ x^{0.6513}$	0.2181
PSSRa	$y = 53.65\ x^{0.8918}$	0.1725

3.3.4.4 Compared with the VI-based method

Wavelengths and Bandwidths of the Sentinel-2 and GF-1 at the same band

GF-1	Central Wavelength	Band width	Resolution	S2	Central Wavelength	Band width	Resolution
B1	485	70	16m	B2	490	65	10m
B2	555	70	16m	B3	560	35	10m
B3	660	60	16m	B4	665	30	10m
B4	830	120	16m	B8	842	115	10m

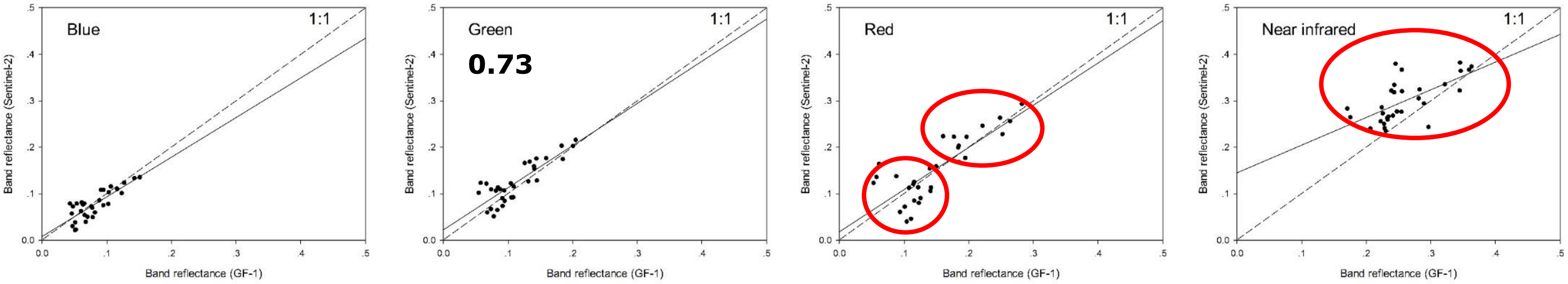

Relationship of the four band reflectance between GF-1 and Sentinel-2 data at the same location

CONTENTS

3.3.5 DISCUSSION

- **Advantages and disadvantages of using machine learning algorithm in AGB estimation in spare vegetation areas**
- **Comparison of Sentinel-2 MSI and GF-1 WFV for AGB estimation in sparse vegetation areas**

0.39 and 0.27

- **Whether the red edge bands in Sentinel-2 MSI could improve the estimation accuracy of AGB in spare vegetation areas?**

B5 and NDI45

- **Variables for AGB estimation in spare vegetation areas**
- **Outlook**

CONTENTS

3.3.6 CONCLUSIONS

The main conclusions of the study are as follows.

(1) Sentinel-2 MSI and GF-1 WFV data could provide substantial support for vegetation monitoring in large areas of the dryland.

(2) Machine learning algorithm could improve the accuracy of sparse vegetation AGB estimation in Otingdag sandy land. Compared with the traditional VI-based method, the R2 of estimated model was increased 0.39 and 0.27 achieved by S2 and GF-1, respectively; And,

(3) combining texture information and red-edge-derived vegetation indices has relatively higher prospects of improving the estimation accuracy of AGB in sparse vegetation areas.

Contents

Data and Method

Net primary productivity（NPP）: Energy utilization model (EC-LUE model) , The accuracy is 75.6%。

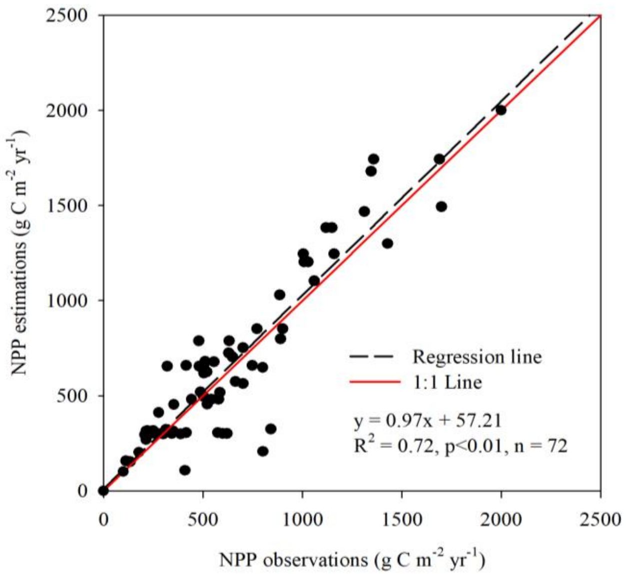

Moisture-Responded NPP（MNPP）

$$MI = \frac{P}{PE}$$

（Recommended by UNCCD， Thornthwait， 1948）

MI: Wetness index; P: Annual precipitation; PE: Contemporaneous potential evapotranspiration.

$$MNPP = \frac{NPP}{MI * 100}$$

Land cover change: Driving force of land degradation

Data and Method

Climate regionalization index of desertification(Thornthwait)

Climatic type	Extreme drought	Dryland			Sub-humid area and humid area
		Dry area	Semi-arid area	Arid dry-humid area	
Wetness index	0-0.05	0.05-0.2	0.2-0.5	0.5-0.65	>0.65

Dryland:

- **Dry area, Semi-arid area, Arid dry-humid area;**
- **Called dry land internationally;**
- Potential areas of desertification.

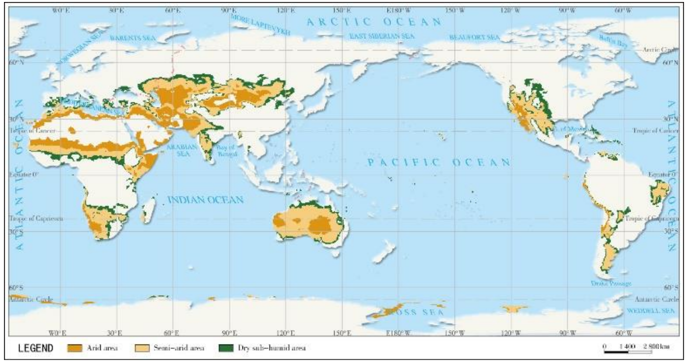

Distribution of the global drylands

Data and Method

NRSCC esa

Remote sensing data
Meteorological data

Data

Land use and cover Ground data

Other auxiliary data

Assessment System for Global Trend of Land Degradation

Indicators and Data

- NPP (GLASS NPP)
- MNPP (NPP/MI)
- MI (Thornthwaite)
- Land cover

Land degrading and improving assessment

Change detection + Grading = Degrading and Improving Assessment

Trend in global land degradation since 2000

Land degradation change detection

Indicators and trends			NPP		
			Sig.↓	No Sig.	Sig.↑
MNPP	Sig.↑	Sig.(MI)↓	Degr.	Fluc.	Impr.
		Others	Degr.	Impr.	Impr.
	Insig.		Degr.	Fluc.	Impr.
	Sig.↓	Sig. (MI)↓	Degr.	Fluc.	Impr.
		Others	Degr.	Degr.	Impr.

Grading for Land degrading and improving assessment

Types	Change level	5-year average change rate of NPP (%)
Degrading	Very sig. degrading	<-9.0
	Sig. degrading	-9.0~-6.0
	Mod. Degrading	-6.0~-3.0
	Sli. Degrading	-3.0~0
Improving	Sli. Improving	0~3.0
	Mod. Improving	3.0~6.0
	Sig. improving	6.0~9.0
	Very sig. improving	>9.0

Trend in Global Land degradation since 2000

The total areas of both degrading and improving processes are basically the same

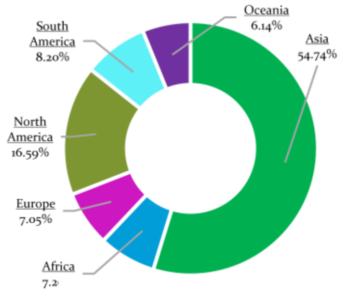

Improving

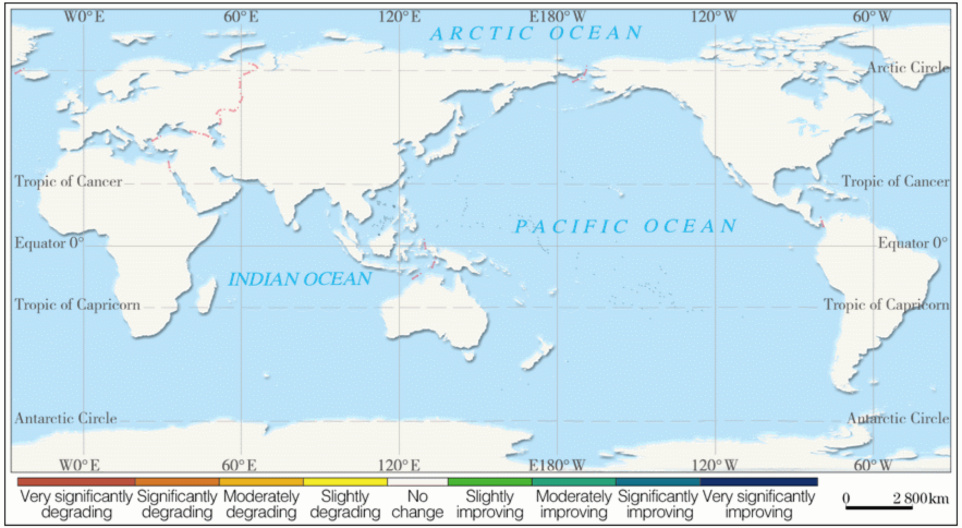

Distribution of global land degrading and improving since 2000

Degrading
Distribution： The southern hemisphere
Area： $1.609\times10^7 km^2$(11.95%)

Improving
Distribution： Asia and North America
Area： $1.648\times10^7 km^2$(12.23%)

Trend in Global Land degradation since 2000

- Africa>South America>Asia>North America>Europe>Oceania
- Moderate>Slight>Significant>Very significant

Degrading

- Asia>North America>South America>Africa>Europe>Oceania
- Moderate>Very significant>Slight>Significant

Improving

- Many traditional land degradation and restoration areas(UNEP, FAO) are reflected.

Degradation: North of the Caspian and Black Seas; Sahel region; Eastern Brazil Plateau, etc.

Improment: China, South Asian Subcontinent, etc.

SDGs

Challenge

→ **Large-scale forest degradation in tropical rainforest areas has occurred since 2000**

Amazon Plain
Congo Basin

A new challenge to the realization of land degradation prevention and control objectives in UN SDGs.

Trend in Global Land degradation since 2000

Distribution of global degrading land of major land cover types

Distribution of global improving land of major land cover types

The areas of both forest degrading and forest improving were the largest among major land cover types

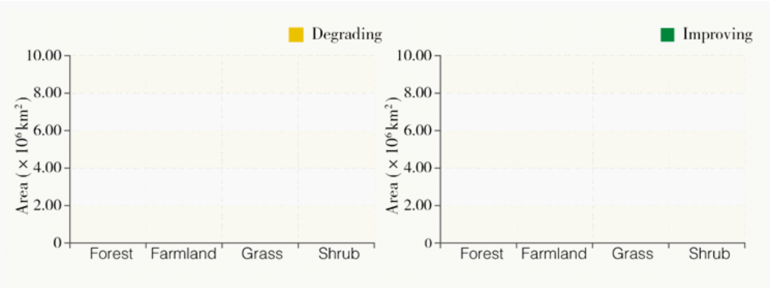

Land degrading and improving areas of major land cover types

Degrading:

Forest(54.21%)>Shrub(17.01%)>Farmland(15.6%)>Grassland(8.34%)

Improving:

Forest(37.35%)>Farmland(25.78%)>Grassland(17.17%)>Shrub(8.74%)

Trend in Global Land degradation since 2000

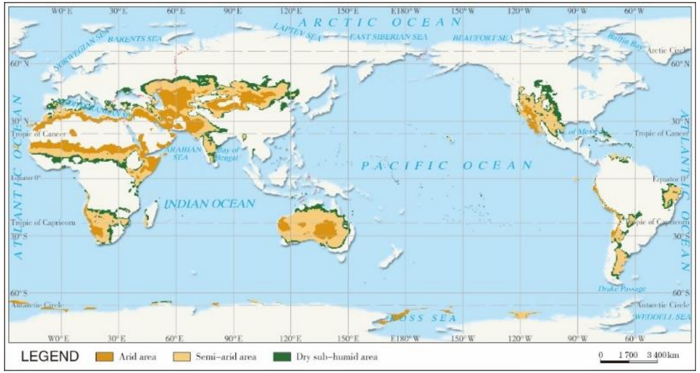

Distribution of global dryland

Distribution of degrading and improving areas of dryland since 2000

Dryland:$3.995\times10^6km^2$(29.65%)

Semi–arid area> Arid area > Dry sub-humid arid area

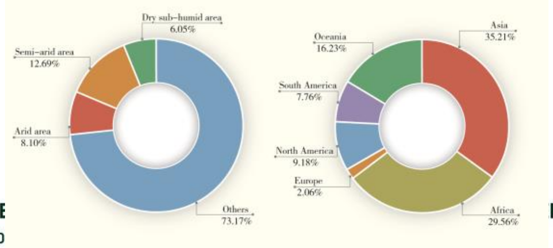

- Degrading process in dryland since 2000: $2.785\times10^6km^2$ (6.97%)
- Mainly distributed in Sahel, East African Plateau, north of the Black and Caspian Seas, Brazil Plateau and southern Africa.

- Improving process in dryland since 2000: $4.341\times10^6km^2$ (10.86%)
- Mainly distributed in Asia, especially in East and South Asia

Land degradation and improvement in key areas

Tropical Forests Degradation

Amazon Plain

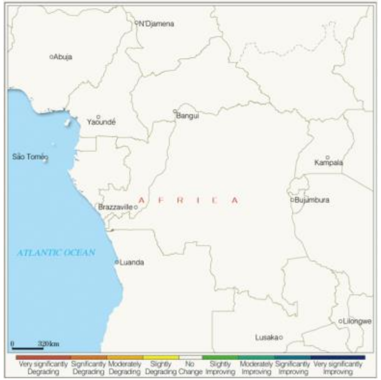

Congo Basin

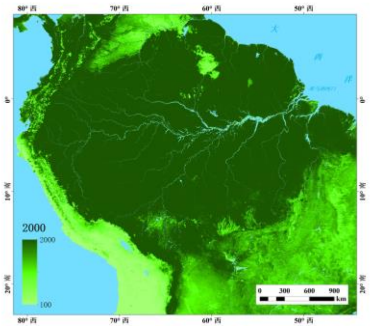

NPP change

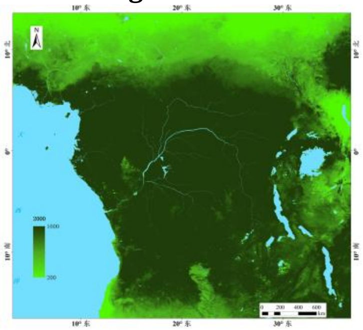

NPP change

- Since 2000, a large area of forest degradation has occurred in tropical rainforest such as the Amazon Plain and the Congo Basin.

- Degrading area of Congo Basin: 3.3×10^6 km^2.
- The area of forest degrading is 2.02×10^6 km^2.

- Degrading area of Amazon Plain: 4.47×10^6 km^2.
- The area of forest degrading is 4.05×10^6 km^2.

Tropical Forests Degradation

- Successive droughts caused by climate warming and El Nino
- Extensive deforestation
- Reclamation
- Frequent fire disturbance in the context of global change

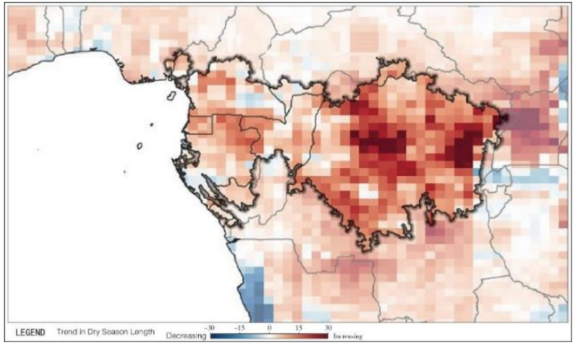

The length of the dry season in the Congo Basin was increasing(Joshua Stevens, 2019)

Amazon Plain

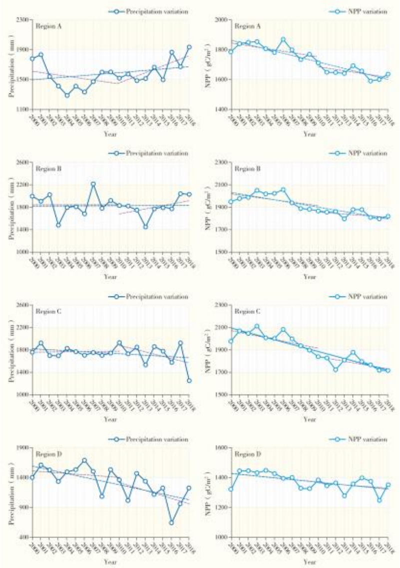

Congo Basin

Precipitation and NPP variations in the Congo Basin and Amazon Plain

Land degradation and improvement in key areas

Land Improvement in Asia

China

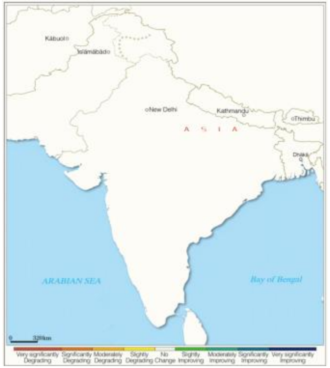

South Asian Subcontinent

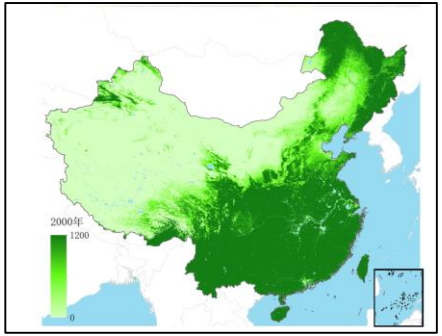

NPP Change in China

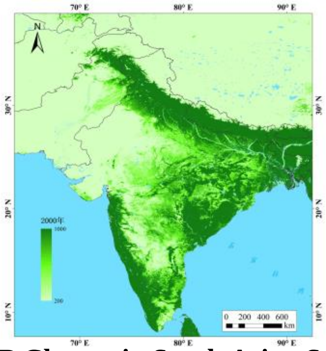

NPP Change in South Asian Subcontinent

- The land improvement in both China and India were significant.
- The contribution rate of these two countries to the global land improvement reached up to 26.78%.
- China contributed almost 20% to the global land improvement.

China(Improving): $3.15\times10^6 km^2$

South Asian Subcontinent : $1.56\times10^6 km^2$

Land degradation and improvement in key areas

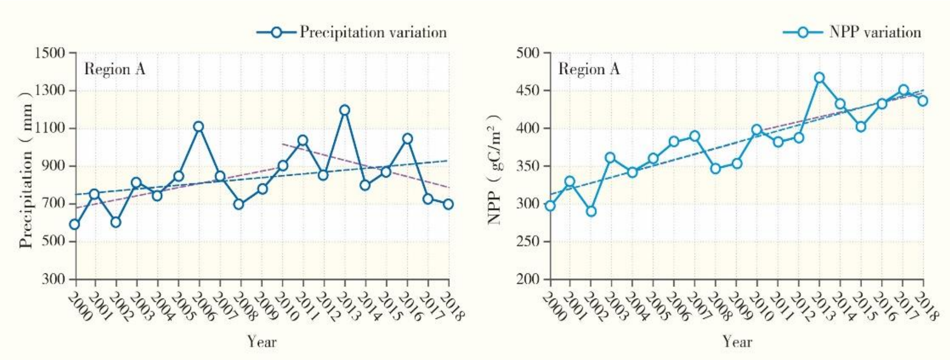

Precipitation and NPP changes in South Asian Subcontinent

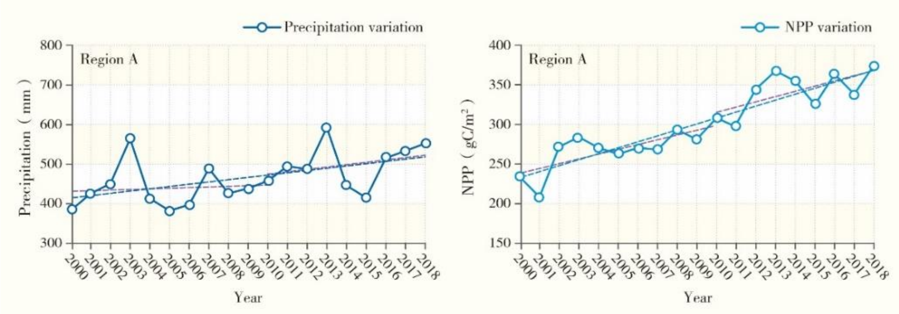

Precipitation and NPP changes in the Loess Plateau of China

- Promote agricultural modernization and improve water irrigation systems, including well-water irrigation system, reservoir irrigation, canal irrigation system.

- The implementation of national-level ecological projects have made the forest area in China increased from 1.75×10^8 ha^2 to 2.20×10^8 ha^2 in the past 20 years

Land degradation and improvement in key areas

Middle Siberia

- Degrading significantly
- Forest degrading area was 1.760×10^5 km^2, occupied 92.2% of total degrading area

Precipitation ↑ NPP ↓

Forest disturbance was serious

Landsat TM/year of 2001

Landsat TM /year of 2019

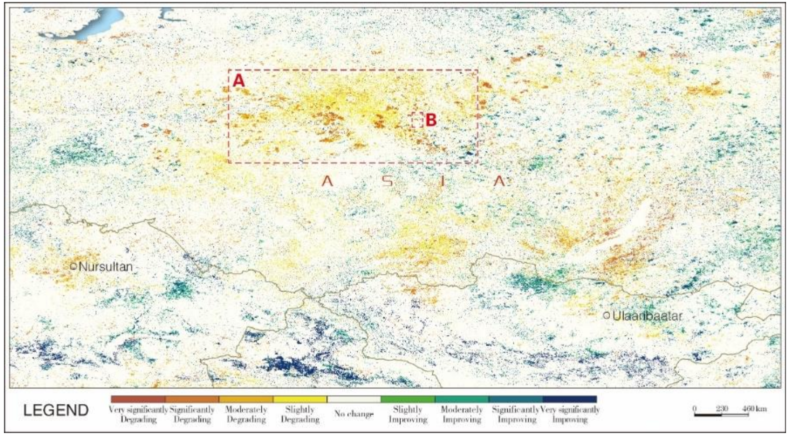

Distribution of land improvement and degradation in middle Siberia

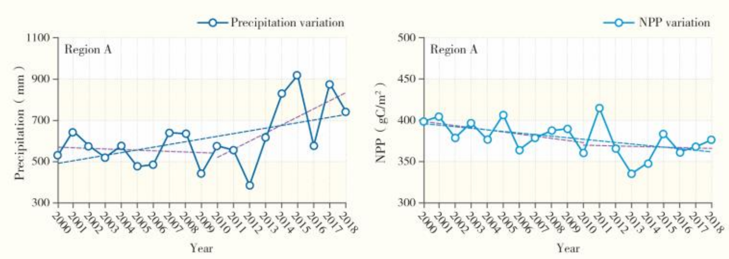

Precipitation and NPP variations in middle Siberia

Land degradation and improvement in key areas

Other key areas

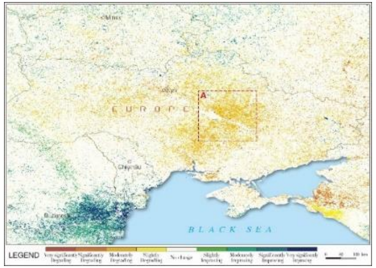

North of the Black Sea

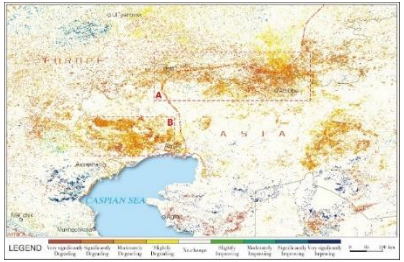

North of the Caspian Sea

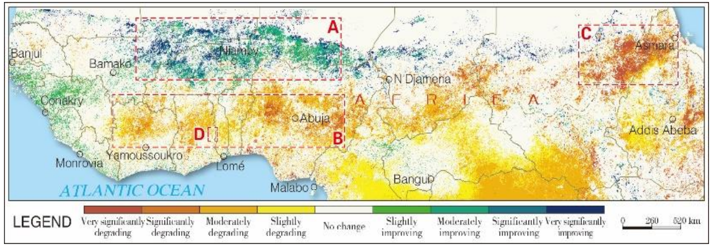

Sahel region

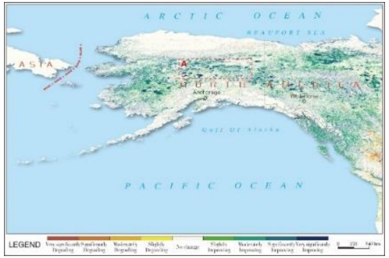

Northwestern North America

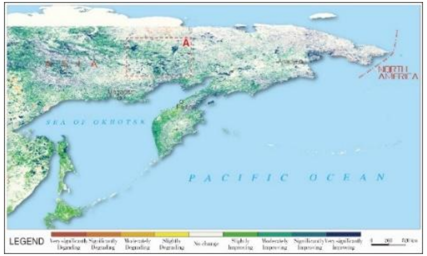

Eastern Siberia

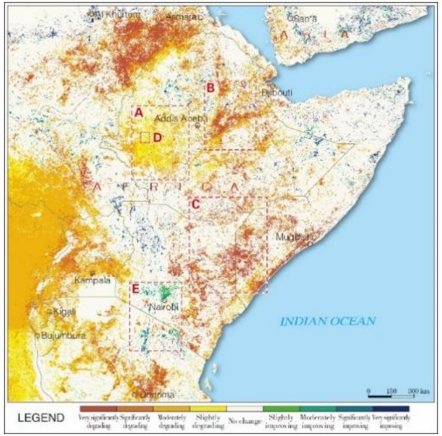

Ethiopian and East African Plateaus

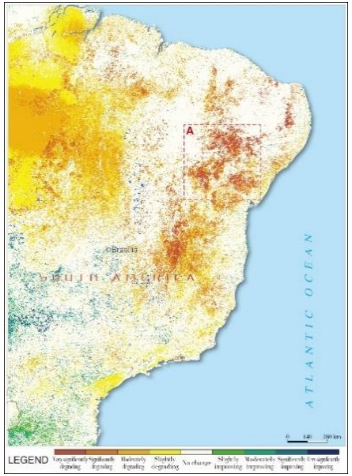

Eastern Brazil Plateau

Conclusions and recommendations

(1) From 2000 to 2018, the processes of global land degradation and improvement occurred simultaneously. The total areas of both processes are basically the same.

(2) The global desertification control has achieved remarkable results due to the implementation of UNCCD.

(3) Large-scaled forest degradation in tropical rainforest areas has occurred since the beginning of this century and it posed a new challenge to the realization of land degradation prevention and control objectives in UN SDGs.

(4) It is recommended that international cooperation in monitoring, assessment and prevention of land degradation should be strengthened.

(5) The successful land degradation management experiences in Asia should be consolidated and extended to other drylands in Africa, South America and other traditional land degradation regions. The best practices will support to the achievements of the United Nations SDGs and Land Degradation Neutrality (LDN).

Thanks for your attention

E-mail:zhihai_gao@163.com; sunbin@ifrit.ac.cn

Phone: 010-62888307;